





Cite this: *RSC Adv.*, 2023, 13, 9281

# Exploring novel derivatives of isatin-based Schiff bases as multi-target agents: design, synthesis, *in vitro* biological evaluation, and *in silico* ADMET analysis with molecular modeling simulations†

Ashraf S. Hassan, <sup>\*a</sup> Nesrin M. Morsy, <sup>a</sup> Wael M. Aboulthana<sup>b</sup> and Ahmed Ragab <sup>\*c</sup>

Recently, scientists developed a powerful strategy called "one drug-multiple targets" to discover vital and unique therapies to fight the most challenging diseases. Novel derivatives of isatin-based Schiff bases 2–7 have been synthesized by the reaction of 3-hydrazino-isatin (1) with aryl aldehydes, hetero-aryl aldehydes, and dialdehydes. The structure of the synthesized derivatives was proved by physical and spectral analysis. Additionally, *in vitro* biological studies were performed, including antioxidant, anti-diabetic, anti-Alzheimer, and anti-arthritis activities. The four derivatives 3b, 5a, 5b, and 5c possess the highest activities. Among the four potent derivatives, compound 5a exhibited the highest antioxidant (TAC = 68.02 ± 0.15 mg gallic acid per g; IRP = 50.39 ± 0.11) and scavenging activities (ABTS = 53.98 ± 0.12% and DPPH = 8.65 ± 0.02 μg mL<sup>-1</sup>). Furthermore, compound 5a exhibited an α-amylase inhibitory percentage of 57.64 ± 0.13% near the acarbose (ACA = 69.11 ± 0.15%) and displayed inhibitor activity of the acetylcholinesterase (AChE) enzyme = 36.38 ± 0.08%. Moreover, our work extended to determining the anti-arthritis effect, and compound 5a revealed good inhibitor activities with very close values for proteinase denaturation (PDI) = 39.59 ± 0.09% and proteinase inhibition (PI) = 36.39 ± 0.08%, compared to diclofenac sodium PDI = 49.33 ± 0.11% and PI = 41.88 ± 0.09%. Additionally, the quantum chemical calculations, including HOMO, LUMO, and energy band gap were determined, and *in silico* ADMET properties were predicted, and their probability was recorded. Finally, molecular docking simulations were performed inside α-amylase and acetylcholinesterase enzymes.

Received 15th January 2023  
Accepted 10th March 2023

DOI: 10.1039/d3ra00297g

rsc.li/rsc-advances

## 1. Introduction

People with diseases have many serious complications that affect many body areas.<sup>1</sup> Diabetes mellitus is a disorder in which the sugar (glucose) level in the blood is elevated. Diabetes mellitus leads to numerous complications, including atherosclerosis which leads to heart attacks and strokes, and blood vessel damage of the eye, then loss of vision (diabetic retinopathy). The other diabetes mellitus complications are damage to the liver, kidney, nerves, and food disorders. Also, gangrene (tissue death), bone infection (osteomyelitis), and reduced immunity against pneumonia and influenza.<sup>2</sup> Alzheimer's

disease is a progressive neurological disorder characterized by degeneration, atrophy, and death of brain cells.<sup>3</sup> Alzheimer's disease is caused by several factors, such as infections, cytotoxicity of amyloid β-protein, increasing age (aging), and genetic characteristics.<sup>4,5</sup> Alzheimer's disease has complications such as depression, hallucinosis (psychiatric disturbances), sleep disturbance, difficulty speaking, pneumonia, constipation or diarrhea, malnutrition or dehydration, and dental problems,<sup>6–8</sup> in addition to cognitive and functional decline.<sup>9</sup> Aging is marked by a progressive loss of human cells and tissues because of genetic and environmental factors and oxidative damage.<sup>10</sup> The free radicals (oxidative damage) are responsible for miscellaneous diseases like cancer, malaria, atherosclerosis, inflammatory diseases, Alzheimer's disease, and diabetes complications.<sup>11,12</sup> Age-related complications are hearing loss, osteoarthritis, diabetes mellitus, depression, Alzheimer's disease, and cardiovascular disease.<sup>13</sup>

Recently, studies, modern research, and bioinformatics analysis proved the close relationship between Alzheimer's disease, diabetes mellitus, oxidative damage, aging, and cardiovascular disease<sup>14–16</sup> (Fig. 1). Numerous drugs on the

<sup>a</sup>Organometallic and Organometalloid Chemistry Department, National Research Centre, Dokki 12622, Cairo, Egypt. E-mail: ashraf\_salmoon@yahoo.com; as.el-salmoon@nrc.sci.eg

<sup>b</sup>Biochemistry Department, Biotechnology Research Institute, National Research Centre, Dokki 12622, Cairo, Egypt

<sup>c</sup>Chemistry Department, Faculty of Science (Boys), Al-Azhar University, Nasr City, Cairo 11884, Egypt. E-mail: ahmed\_ragab7@gmail.com; Ahmed\_ragab@azhar.edu.eg

† Electronic supplementary information (ESI) available. See DOI: <https://doi.org/10.1039/d3ra00297g>



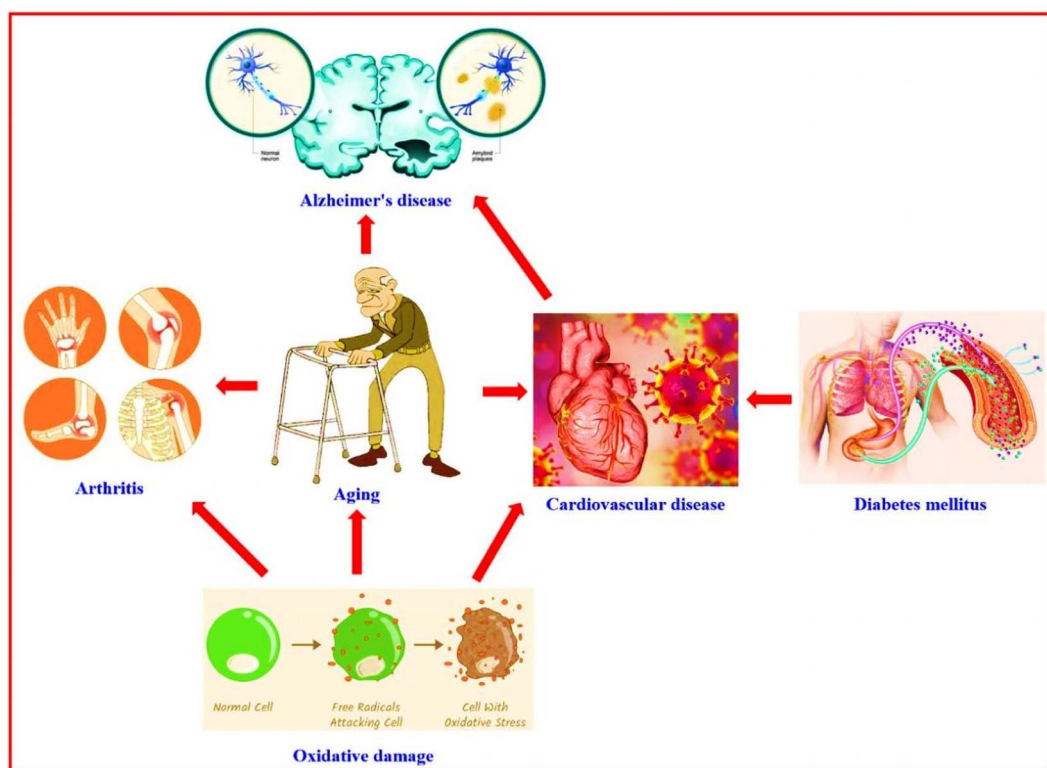


Fig. 1 Illustration of the relationship between diseases.

market target a single disease; therefore, these drugs are working on one target “one drug-one target”. A patient with various diseases suffers a problem when taking more than one drug at the same time or near times between doses. This problem may be caused by interference for some drugs that don't work effectively against disease and, in some cases, don't work with each other (antagonistic properties appear) and in some cases may don't work completely. Consequently, research cooperation continues between scientists for the chemical studies and biological applications of the nitrogen heterocycle compounds in the hope of finding a new drug with multi-biologically target “one drug-multiple target”. This is one of the efficient strategies for discovering novel categories of therapeutics or the development of drugs to face and fight against the most challenging diseases, especially after the Covid-19 pandemic and appearing numerous healthy problems complicated.<sup>17–22</sup>

In recent decades, the isatin (2,3-dioxindole) (**I**) molecule has attracted the concern of scientists for its potent biological and therapeutic applications.<sup>23–25</sup> Also, isatin derivatives have numerous distinct biological activities. Ethyl 4-chlorobenzoyl hydrazono-2-oxoindolin-1-yl acetate **II** is biologically active as a powerful *in vitro* inhibitor for an  $\alpha$ -amylase enzyme (anti-diabetic agent).<sup>26</sup> The isatin thiosemicarbazone derivative **III** acts as an inhibitor against acetylcholinesterase enzyme *in vitro* (anti-Alzheimer agent).<sup>27</sup> Additionally, 2-oxoindolin-3-ylidene-pyrrolidine-3-carbohydrazide derivative **IV** possessed a high ability to iron reducing power (antioxidant agent).<sup>28</sup> Moreover,

the morpholinosulfonyl-2-oxoindolin-3-ylidene compound **V** showed a broad-spectrum and potent anticancer activity against HepG-2, HCT-116, and MCF-7 cell lines.<sup>29</sup> Besides, the derivative 1*H*-pyrazol-4-yl-5-(morpholinosulfonyl)indolin-2-one **VI** exposures antibacterial activity and is a potent inhibitor of *S. aureus* DNA gyrase.<sup>30</sup> Additionally, some clinical drugs incorporate isatin moiety as nintedanib®, which acts as a tyrosine kinases inhibitor and a lung cancer treatment,<sup>31</sup> methisazone® that act as an mRNA inhibitor, protein synthesis, and an antiviral drug;<sup>32</sup> and sunitinib® is act as receptor tyrosine kinase (RTK) inhibitor and renal cell carcinoma (RCC) therapy<sup>33</sup> (Fig. 2). On the other hand, the Schiff bases linked to a heterocyclic scaffold displayed interesting and numerous biological activities. Schiff base associated with 1,2,4-triazole **VII** displayed highly anti-bacterial activity against *Halomonas salina* and inhibitor activity against the two enzymes butyrylcholinesterase and acetylcholinesterase (enzymes of anti-Alzheimer disease).<sup>34</sup> Further, the Schiff base tethered pyrazole scaffold **VIII** demonstrated an inhibitory impact *in vitro* against *B. subtilis* DNA gyrase and dihydrofolate reductase (enzymes of bacterial infection)<sup>35</sup> (Fig. 2).

In view of our scientific team targets in medicinal chemistry based on bioactive heterocyclic compounds<sup>36–42</sup> and the previous-mentioned facts about the relationship between various diseases, applications of isatin derivatives, and various activities of Schiff bases tethered with a heterocyclic scaffold. Hence, the present study aims to explore isatin-based Schiff bases (azomethine) as multi-target agents. Consequently, we



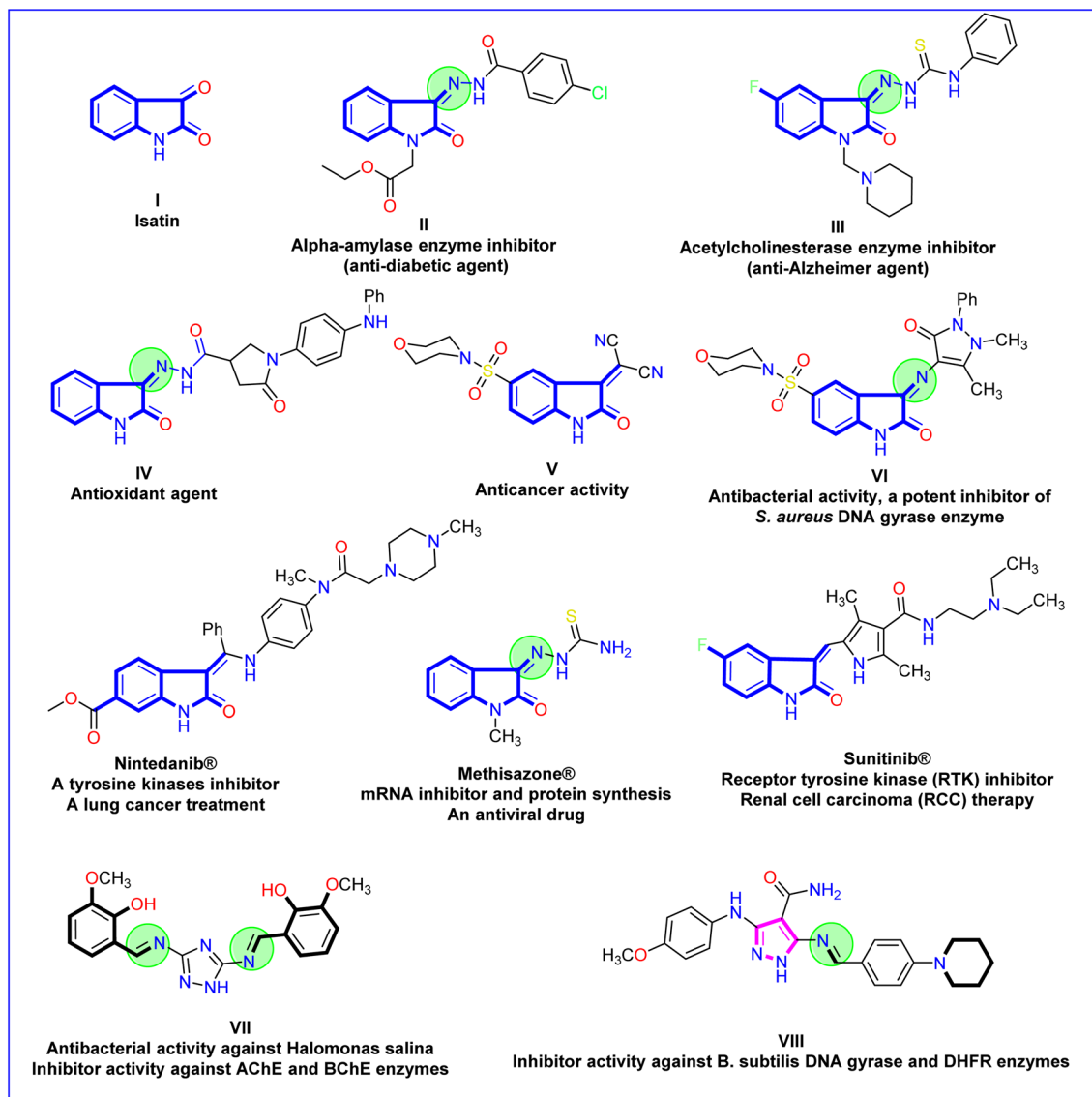


Fig. 2 Chemical structures of bioactive isatin derivatives, isatin drugs, and Schiff bases associated with heterocyclic scaffold.

synthesized a new series of isatin-based azomethine derivatives **2a** and **2b**, isatin-azomethine-aryl azo **3a–d**, isatin-azomethine-heterocyclic moiety **4**, **5a–c**, and **6**, and *bis*-Schiff bases based on isatin **7a** and **7b**. All the synthesized isatin-based Schiff bases structures were confirmed and evaluated for their antioxidant, anti-diabetic, anti-Alzheimer, and anti-arthritic activities. Finally, the structure–activity relationship study, the Quantum chemical calculations, the molecular docking simulation, and *in silico* ADMET properties of the most potent isatin-based Schiff bases (azomethine) **3b** and **5a–c** were predicted and studied.

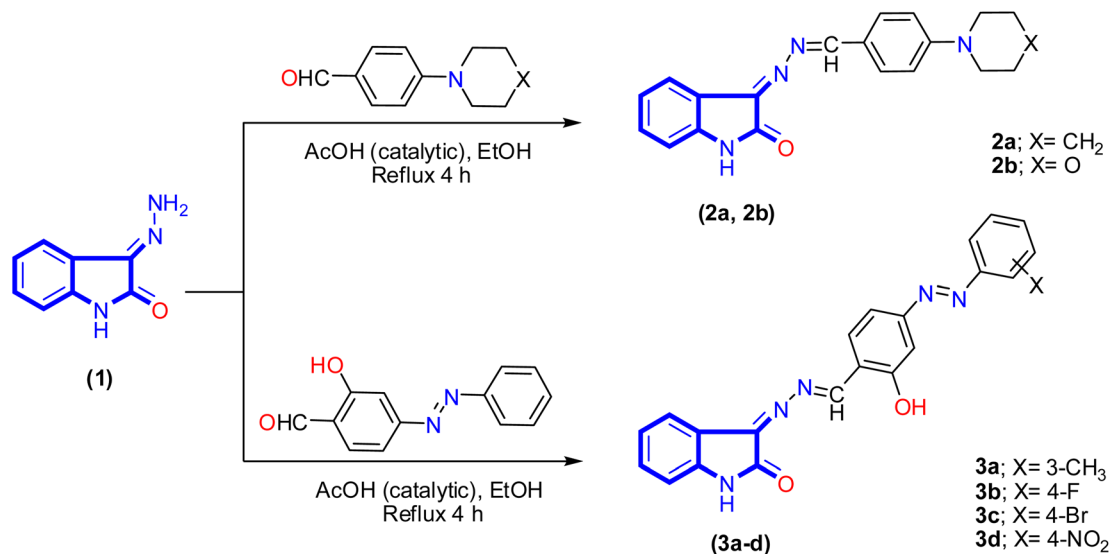
## 2. Results and discussion

### 2.1. Chemistry

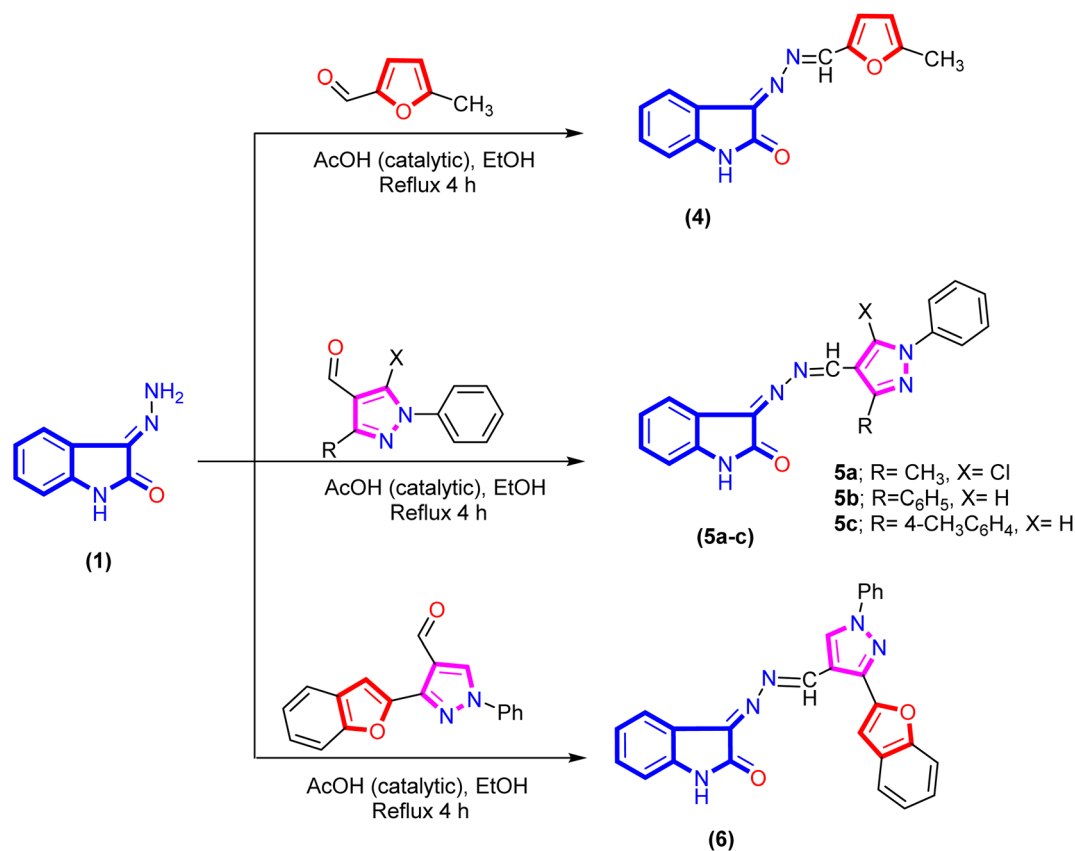
A new series of isatin-based Schiff bases **2a**, **2b**, **3a–d**, **4**, **5a–c**, **6**, **7a**, and **7b** were synthesized based on a reaction of 3-hydrazonoindolin-2-one (**1**) that was previously prepared<sup>43</sup> with

different formyl derivatives, and the structures of the newly designed compounds are outlined in Schemes 1–3. Our research was designed by reaction of 3-hydrazonoindolin-2-one (**1**) with different formyl cores as series 1 containing aromatic formyl containing aliphatic or azo (N=N) group (Scheme 1), series 2 involved heterocyclic formyl based on pyrazole or furane core (Scheme 2), and series 3 including bis-formyl derivatives (Scheme 3).

Firstly, the isatin-based azomethine derivatives **2a**, **2b**, and isatin-azomethine-arylazo derivatives **3a–d** were synthesized *via* the reaction of 3-hydrazonoindolin-2-one (**1**) with aryl aldehydes (namely: 4-(piperidin-1-yl)benzaldehyde, 4-morpholino-benzaldehyde, and 2-hydroxy-4-((4-substituted-phenyl)azo) benzaldehyde) in ethanol (solvent)/glacial acetic acid (catalytic) under reflux conditions, where the product obtained after cooling (Scheme 1). Spectral data and elemental analysis confirmed the structures of the synthesized isatin-based azomethine derivatives **2a**, **2b**, and **3a–d**.



Scheme 1 Synthesis of isatin-based azomethine 2a, 2b, and isatin-azomethine-aryldiazo 3a–d.

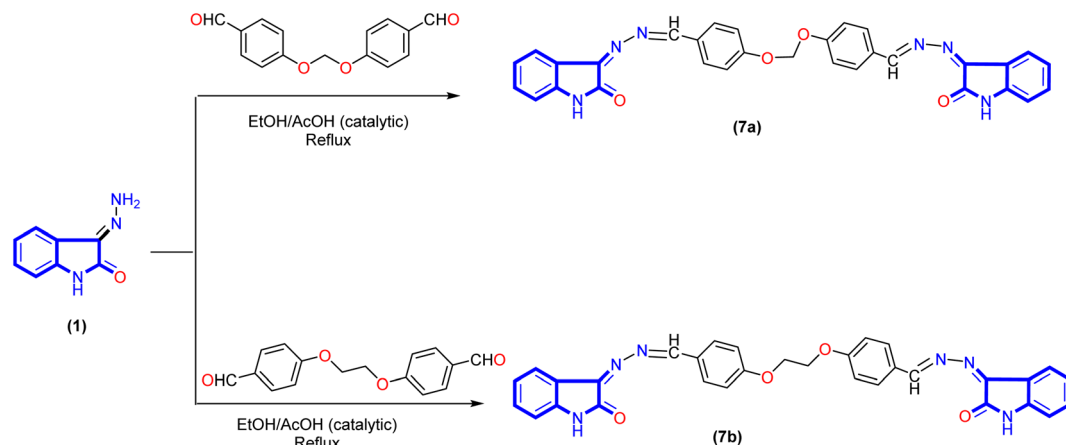


Scheme 2 Synthesis of isatin-azomethine-heterocyclic 4, 5a–c, and 6.

The IR spectrum of 3-((4-morpholino/pipridino-benzylidene)hydrazono)indolin-2-one **2a** and **2b** displayed various bands related to functional groups as NH, carbonyl (C=O), and azomethine (C=N) groups ranging between 3171–3193, 1723–1725,

and 1605–1611 cm<sup>−1</sup>, respectively. Similarly, the azo-aryl-Schiff bases **3a–d** exhibited bands ranging between 3429–3440, 3159–3200, 1715–1726, and 1618–1620 cm<sup>−1</sup> assigned to OH, NH, C=O, and C=N groups, respectively. The <sup>1</sup>H NMR spectrum





Scheme 3 Synthesis of bis-Schiff bases based on isatin 7a and 7b.

analysis of compound **2b** appeared the morpholinyl moiety as two signals with the integration of four for each single and displayed as multiplet between  $\delta$  3.27–3.29 ppm and singlet signal at  $\delta$  3.71 ppm. Besides, two singlet signals at  $\delta$  8.58 and 10.75 ppm correspond to azomethine and NH proton of the isatin derivative. The aromatic protons (8 protons) range between  $\delta$  6.86–8.11 ppm appearing as four doublets signals for six protons and two triplet signals for two protons. Moreover, the  $^{13}\text{C}$  NMR spectrum of compound **2b** revealed two signals at  $\delta$  47.42 and 66.40 ppm for the four carbon atoms of morpholinyl moiety, the aromatic and azomethine carbon atoms range from  $\delta$  111.18 to 164.17 ppm, and carbonyl carbon at  $\delta$  165.54 ppm. In the same way, the  $^1\text{H}$  NMR spectrum analysis of salicylaldehyde derivatives **3a–d** showed significant signals at  $\delta$  8.81–8.87, 10.90–10.97, and 11.03–12.56 ppm attributed to azomethine proton, phenolic hydroxyl group, and NH of isatin derivative, respectively. Moreover, in the case of salicylaldehyde derivative **3a** the signal that appeared at  $\delta$  2.42 ppm confirmed three protons presented in the methyl group. All the above-mentioned spectroscopic data confirmed the structure of the proposed compounds.

Furthermore, refluxing 3-hydrazonoindolin-2-one (**1**) with hetero-aryl aldehydes under the same reaction conditions afforded the corresponding 3-(((hetero-aryl)methylene)hydrazono)-indolin-2-one derivatives **4**, **5a–c**, and **6** (Scheme 2). Additionally, the Schiff base of isatin hybrid heterocyclic core structures **4–6** were confirmed by spectral data. The IR spectrum of compound **5c** exhibited the absence of forked bands for the amino group (corresponding to hydrazone) and the presence of other stretching bands at 3202, 1727, and 1615  $\text{cm}^{-1}$  attributed to NH, C=O, and C=N groups, respectively. The  $^1\text{H}$  NMR spectrum of compound **4** exhibited three significant signals at  $\delta$  2.38, 8.53, and 10.87 ppm, which are assignable to methyl protons, azomethine proton, and NH proton, respectively. In addition, an increasing number of aromatic protons with two doublet signals at  $\delta$  6.50 and 7.30 ppm with coupling constant ( $J = 3.7$  Hz) corresponding to furane core. Meanwhile, the  $^1\text{H}$  NMR spectrum of the isatin-based azomethine-heterocyclic derivative **5c** distinguished by four singlets signals at  $\delta$  2.36,

8.69, 9.30, and 10.78 ppm for the methyl group, azomethine proton, proton of the pyrazole H-5, and NH proton of the isatin ring, respectively. Besides, aromatic protons of the isatin ring appeared as two doublets at  $\delta$  6.83 and 7.90 ppm with coupling constant ( $J = 7.8$  and 7.4 Hz) and two triplet signals at  $\delta$  6.88 and 7.40 ppm. Moreover, the other nine protons of the two aromatic rings (phenyl and 4-methylphenyl) emerged at  $\delta$  7.30–7.34, 7.56, 7.62, and 8.02 as one multiplet, one triplet, and two doublets ( $J = 8.0$  and 8.1 Hz) integrated for 3H, 2H, and 4H. Further, the  $^{13}\text{C}$  NMR spectrum of azomethine derivative **5c** exhibited two peaks at  $\delta$  21.00 and 164.94 ppm for the carbon atoms of the methyl ( $\text{CH}_3$ ) and carbonyl ( $\text{C}=\text{O}$ ) groups. In addition, peaks of the aromatic and azomethine carbon atoms (the twenty-three carbons) were marked between  $\delta$  110.53–157.25 ppm.

*Bis*-Schiff bases are famous for their antitumor, antioxidant, antiglycation, antibacterial, and antiviral activities.<sup>44–46</sup> Also, act as inhibitors of enzymes such as  $\alpha$ -glucosidase,<sup>47</sup> butyrylcholinesterase, and acetylcholinesterase.<sup>48</sup> As shown in Scheme 3, the reaction was readily extended to synthesize a new *bis*-Schiff base by reaction of 3-hydrazonoindolin-2-one (**1**) with various *bis*-aldehyde. Spectral data (IR,  $^1\text{H}$  NMR, and  $^{13}\text{C}$  NMR) and elemental analysis confirmed the structures of all newly synthesized compounds **7a** and **7b**.

Regarding the IR spectra of *bis*-Schiff bases **7a** and **7b** displayed high similarity by displaying bands around  $\nu$  1605–1607, 1725–1730, and 3199–3204  $\text{cm}^{-1}$  corresponding to C=N, C=O, and NH groups, respectively. The  $^1\text{H}$  NMR spectrum of compound **7a** is characterized by a singlet signal at  $\delta$  6.03 ppm related to the methylene group, two signals at  $\delta$  8.58 and 8.61 ppm for two azomethine protons, and a signal at  $\delta$  10.81 ppm for two NH protons. Besides, the aromatic protons displayed between  $\delta$  6.85–7.96 ppm for sixteen protons. The  $^{13}\text{C}$  NMR spectrum of *bis*-Schiff base **7a** exhibited two peaks at  $\delta$  89.38 and 164.67 ppm for the methylene carbon atom (1C,  $\text{CH}_2$ ) and carbonyl atoms (2C,  $\text{C}=\text{O}$ ), respectively. In addition, the twenty-six aromatic carbon with the two azomethine carbon atoms ranged from  $\delta$  110.79 to 160.94 ppm (the twenty-eight carbon atoms). Finally, all the newly synthesized Schiff bases



were characterized by forming a new azomethine proton, as represented in the discussion and Experimental section.

## 2.2. *In vitro* biological activities and SAR analysis

**2.2.1. Antioxidant activities.** Oxidative stress in living organisms leads to aging and a series of chronic diseases. The oxidative damage degree can be controlled through antioxidants which can scavenge free radicals or prevent oxidation reactions.<sup>49</sup> According to this, all isatin-based Schiff bases **2a**, **2b**, **3a–d**, **4**, **5a–c**, **6**, **7a**, and **7b** were studied by evaluating their antioxidant activities using four different antioxidant assays. The results of antioxidant activities, such as iron-reducing power (IRP), total antioxidant capacity (TAC), and the scavenging activities against 2,2'-azinobis-(3-ethylbenzothiazoline-6-sulfonic acid) (ABTS) and 1,1-diphenyl-2-picryl-hydrazyl (DPPH) radicals were listed in Table 1. The effect of structural modification of the newly isatin-based Schiff bases 2–7 were evaluated on the antioxidant activity compared to ascorbic acid.

Firstly, the synthesized derivatives incorporating azomethine-isatin Schiff base demonstrated various degrees of antioxidant activity represented by iron-reducing power (IRP =  $\mu\text{g mL}^{-1}$ ) and total antioxidant capacity (TAC = mg gallic acid per g). The 3-(((5-chloro-3-methyl-1H-pyrazol-4-yl)methylene)hydrazono)indolin-2-one derivative **5a** recorded the best antioxidant activity among all the tested derivatives with the strongest reducing power (IRP =  $50.39 \pm 0.11 \mu\text{g mL}^{-1}$ ) and highest antioxidant capacity (TAC =  $68.02 \pm 0.15 \text{ mg gallic acid per g}$ ) and that may be related to the presence of methyl group and chlorine atom at position three and five in pyrazole moiety (electron delocalized aromatic nucleus).

As can be seen in Table 1, the other two pyrazole derivatives **5b** (IRP =  $48.92 \pm 0.11 \mu\text{g mL}^{-1}$  and TAC =  $66.03 \pm 0.14 \text{ mg gallic acid per g}$ ) and **5c** (IRP =  $49.41 \pm 0.11 \mu\text{g mL}^{-1}$  and TAC =  $66.70 \pm 0.15 \text{ mg gallic acid per g}$ ), showed nearly equipotent

with a slight difference in antioxidant activity. In addition, introducing a heterocyclic ring with one hetero-atom as furan instead of pyrazole doesn't enhance the activity and the antioxidant activities may be related to the presence of two hetero-atoms in five-ring as pyrazole ring that showed effected in the antioxidant activity. To our surprise, replacing of aryl group at C3 of pyrazole to benzo[*b*]furan as compound **6** causes dramatically decrease for (IRP =  $17.40 \pm 0.04 \mu\text{g mL}^{-1}$  and TAC =  $30.70 \pm 0.07 \text{ mg gallic acid per g}$ ) compared with 3-arylpyrazole derivatives **5b** and **5c**, indicating that the presence of furan fused to benzene ring to form benzo[*b*]furan decrease antioxidant activity by nearly from 0.25 to 0.50 of its activity.

Furthermore, compounds **2a** and **2b**, which are Schiff bases with piperidinyl and morpholinyl derivatives showed moderate antioxidant activity with IRP values of ( $19.93 \pm 0.04$  and  $20.12 \pm 0.04 \mu\text{g mL}^{-1}$ ) and TAC values of ( $35.59 \pm 0.08$  and  $35.92 \pm 0.08 \text{ mg gallic acid per g}$ ), respectively. Moreover, forming new Schiff bases that bear phenolic hydroxyl group as salicylamide derivatives **3a–d** with a different substituent at the *para* position of the azoaryl group don't enhance the antioxidant activity compared to other derivatives, except with compound **3b** that bears (4-fluorophenyl)azo group at C5 of salicylamide derivative **3b** with IRP values of ( $47.87 \pm 0.10 \mu\text{g mL}^{-1}$ ) and TAC values of ( $64.62 \pm 0.14 \text{ mg gallic acid per g}$ ). The values of IRP and TAC of *bis*-compounds exhibited moderate activity, indicating an increase in the isatin nucleus and the presence of new ether linkage in the structure don't affect activity.

The scavenging activities using the ABTS and DPPH radicals were evaluated for isatin-based Schiff bases, and the results obtained ranged from  $23.27 \pm 0.05$  to  $53.98 \pm 0.12\%$  compared with ascorbic acid ( $39.09 \pm 0.09\%$ ) for ABTS. Moreover, the interaction of the synthesized compounds with stable free radical DPPH indicated radical scavenging ability represented by  $\text{IC}_{50}$  values ranging from  $8.65 \pm 0.02$  to  $8.65 \pm 0.02 \mu\text{g mL}^{-1}$  in comparison to ascorbic acid ( $4.05 \pm 0.01 \mu\text{g mL}^{-1}$ ). It was

**Table 1** Total iron reducing power, total antioxidant capacity, and free radicals scavenging activities of isatin-based Schiff bases **2a**, **2b**, **3a–d**, **4**, **5a–c**, **6**, **7a**, and **7b**

Isatin-based Schiff bases	Antioxidant activities		Free radical scavenging activities	
	IRP ( $\mu\text{g mL}^{-1}$ )	TAC (mg gallic acid per g)	ABTS (%)	DPPH ( $\text{IC}_{50} \mu\text{g mL}^{-1}$ )
<b>2a</b>	$19.93 \pm 0.04$	$35.59 \pm 0.08$	$28.78 \pm 0.06$	$15.10 \pm 0.03$
<b>2b</b>	$20.12 \pm 0.04$	$35.92 \pm 0.08$	$29.05 \pm 0.06$	$14.96 \pm 0.03$
<b>3a</b>	$21.13 \pm 0.05$	$37.74 \pm 0.08$	$30.51 \pm 0.07$	$14.25 \pm 0.03$
<b>3b</b>	$47.87 \pm 0.10^a$	$64.62 \pm 0.14^a$	$51.28 \pm 0.11^a$	$9.11 \pm 0.02^a$
<b>3c</b>	$20.93 \pm 0.05$	$37.36 \pm 0.08$	$30.21 \pm 0.07$	$14.39 \pm 0.03$
<b>3d</b>	$22.81 \pm 0.05$	$40.72 \pm 0.09$	$32.93 \pm 0.07$	$13.20 \pm 0.03$
<b>4</b>	$18.63 \pm 0.04$	$33.26 \pm 0.07$	$26.90 \pm 0.06$	$16.16 \pm 0.04$
<b>5a</b>	$50.39 \pm 0.11^a$	$68.02 \pm 0.15^a$	$53.98 \pm 0.12^a$	$8.65 \pm 0.02^a$
<b>5b</b>	$48.92 \pm 0.11^a$	$66.03 \pm 0.14^a$	$52.41 \pm 0.11^a$	$8.91 \pm 0.02^a$
<b>5c</b>	$49.41 \pm 0.11^a$	$66.70 \pm 0.15^a$	$52.93 \pm 0.12^a$	$8.82 \pm 0.0^a$
<b>6</b>	$17.40 \pm 0.04$	$30.70 \pm 0.07$	$23.27 \pm 0.05$	$18.63 \pm 0.04$
<b>7a</b>	$20.74 \pm 0.05$	$37.03 \pm 0.08$	$30.76 \pm 0.07$	$15.04 \pm 0.03$
<b>7b</b>	$20.94 \pm 0.05$	$37.40 \pm 0.08$	$31.07 \pm 0.07$	$14.89 \pm 0.03$
Ascorbic acid	—	—	$39.09 \pm 0.09$	$4.05 \pm 0.01$

<sup>a</sup> Denotes the most effective compound, values were calculated from three replicates and expressed as mean  $\pm$  SE.



found that four isatin-based Schiff bases have the best ABTS and DPPH values, where the salicylamide derivative **3b** showed (ABTS =  $51.28 \pm 0.11\%$  and DPPH =  $9.11 \pm 0.02 \mu\text{g mL}^{-1}$ ), and the other three Schiff bases with pyrazole heterocyclic moiety as **5a** (ABTS =  $53.98 \pm 0.12\%$  and DPPH =  $8.65 \pm 0.02 \mu\text{g mL}^{-1}$ ), **5b** (ABTS =  $52.41 \pm 0.11\%$  and DPPH =  $8.91 \pm 0.02 \mu\text{g mL}^{-1}$ ), and **5c** (ABTS =  $52.93 \pm 0.12\%$  and DPPH =  $8.82 \pm 0.02 \mu\text{g mL}^{-1}$ ), and the order of activity as the most potent represented in the range of **5a** > **5c** > **5b** > **3b**.

As represented in Table 1, Schiff bases containing in the side chain amine derivatives **2a**, **2b**, and azo-aryl group **3a–d** displayed weak to moderate free radical scavenging activities (ABTS and DPPH). This low activity may be related to the disability of amine (piperidinyl and morpholinyl) and azo-aryl groups (4-methyl, 4-bromo, and 4-nitro) to catch radicals, except **3b** derivatives that indicate the presence of fluorine atom as strong electron withdrawing group that helps the aromatic aryl group permits the trapping of free radical. Additionally, the introduction of heterocyclic rings to the azomethine group showed enhancement of the antioxidant activity, especially with the pyrazole nucleus that displayed importance for antioxidant activity as represented in compounds **5a–c**. The 3-(((1*H*-pyrazol-4-yl)methylene)hydrazono)indolin-2-one derivatives **5a–c** demonstrated excellent ABTS values between ( $52.41 \pm 0.11$  to  $53.98 \pm 0.12\%$ ) and good DPPH values  $\text{IC}_{50}$  ranging between ( $8.65 \pm 0.02$  to  $8.91 \pm 0.02 \mu\text{g mL}^{-1}$ ) compared with 3-(((5-methylfuran-2-yl)methylene)hydrazono)-indolin-2-one (**4**) with ABTS (%) =  $26.90 \pm 0.06$  and DPPH ( $\text{IC}_{50}$  =  $16.16 \pm 0.04 \mu\text{g mL}^{-1}$ ) and 3-(((3-(benzofuran-2-yl)-1*H*-pyrazol-4-yl)methylene)hydrazono)indolin-2-one **6** with ABTS (%) =  $23.27 \pm 0.05$  and DPPH ( $\text{IC}_{50}$  =  $18.63 \pm 0.04 \mu\text{g mL}^{-1}$ ). The structure–activity relationship (SAR) revealed that the pyrazole core has antioxidant activity higher than furan and pyrazole containing benzo

[*b*]furan group and this better activity may be due to the efficiency of the trapping. Even though the Schiff base with heterocyclic core **4–6** exhibited good antioxidant activity compared with other synthesized derivatives, but ascorbic acid remained the best activity with ABTS (%) =  $39.09 \pm 0.09$  and DPPH ( $\text{IC}_{50}$  =  $4.05 \pm 0.01 \mu\text{g mL}^{-1}$ ).

Furthermore, the *bis*-Schiff bases **7a** and **7b** exhibited moderate activity, and the presence of ethane-1,2-dioyl as a linker between two Schiff bases demonstrated slightly higher free radical scavenging activities with ABTS (%) =  $31.07 \pm 0.07$  and low DPPH ( $\text{IC}_{50}$  =  $14.89 \pm 0.03 \mu\text{g mL}^{-1}$ ) compared with methane-1,1-dioyl derivative activities (ABTS =  $30.76 \pm 0.07\%$  and DPPH  $\text{IC}_{50}$  =  $15.04 \pm 0.03 \mu\text{g mL}^{-1}$ ). Finally, it can be concluded that among the isatin-based Schiff bases **2a**, **2b**, **3a–d**, **4**, **5a–c**, **6**, **7a**, and **7b** introducing the pyrazole motif as **5a–c** or strong electron-withdrawing group to azo-salicylamide moiety as **3b** are more effective antioxidants than others cores or substituents.

### 2.2.2. Anti-diabetic activity ( $\alpha$ -amylase enzyme inhibition).

The  $\alpha$ -amylase enzyme is responsible for the breakdown of starch and oligosaccharides. As a result,  $\alpha$ -amylase enzyme inhibition is one of the important techniques for diabetes mellitus therapy.<sup>50</sup> Accordingly, the anti-diabetic activity of isatin-based Schiff bases **2a**, **2b**, **3a–d**, **4**, **5a–c**, **6**, **7a**, and **7b** was estimated by determining the ability of these derivatives to inhibit an  $\alpha$ -amylase enzyme.<sup>51</sup> Acarbose was used as a standard reference ( $\alpha$ -amylase inhibition =  $69.11 \pm 0.15\%$ ).

As described in Table 2, all compounds exhibited moderate to good  $\alpha$ -amylase inhibition (%), ranging from  $26.97 \pm 0.06$  to  $57.64 \pm 0.13\%$ . Among the tested compounds, the Schiff base with pyrazole motif **5a–c** and salicylamide containing azo-aryl with *para*-fluoro atom **3b** are relatively more potent than other derivatives. The result of the anti-diabetic activity (Table 2)

Table 2 Anti-diabetic, anti-Alzheimer, and anti-arthritis biological activities of isatin-based Schiff bases **2a**, **2b**, **3a–d**, **4**, **5a–c**, **6**, **7a**, and **7b**

Isatin-based Schiff bases	Anti-diabetic activity	Anti-Alzheimer's activity	Anti-arthritis activity	
	$\alpha$ -Amylase inhibition (%)	Acetylcholinesterase (AChE) inhibition (%)	Proteinase denaturation (%)	Inhibition of proteinase (%)
<b>2a</b>	$29.84 \pm 0.06$	$17.14 \pm 0.04$	$19.23 \pm 0.04$	$17.03 \pm 0.04$
<b>2b</b>	$30.12 \pm 0.07$	$17.30 \pm 0.04$	$19.40 \pm 0.04$	$17.19 \pm 0.04$
<b>3a</b>	$31.64 \pm 0.07$	$18.17 \pm 0.04$	$20.38 \pm 0.04$	$18.06 \pm 0.04$
<b>3b</b>	$54.76 \pm 0.12^a$	$34.56 \pm 0.08^a$	$37.61 \pm 0.08^a$	$34.57 \pm 0.08^a$
<b>3c</b>	$31.33 \pm 0.07$	$17.99 \pm 0.04$	$20.18 \pm 0.04$	$17.88 \pm 0.04$
<b>3d</b>	$34.15 \pm 0.07$	$19.61 \pm 0.04$	$22.00 \pm 0.05$	$19.45 \pm 0.04$
<b>4</b>	$27.89 \pm 0.06$	$16.02 \pm 0.03$	$17.97 \pm 0.04$	$15.92 \pm 0.03$
<b>5a</b>	$57.64 \pm 0.13^a$	$36.38 \pm 0.08^a$	$39.59 \pm 0.09^a$	$36.39 \pm 0.08^a$
<b>5b</b>	$55.96 \pm 0.12^a$	$35.32 \pm 0.08^a$	$38.44 \pm 0.08^a$	$35.33 \pm 0.08^a$
<b>5c</b>	$56.52 \pm 0.12^a$	$35.68 \pm 0.08^a$	$38.82 \pm 0.08^a$	$35.69 \pm 0.08^a$
<b>6</b>	$26.97 \pm 0.06$	$15.75 \pm 0.03$	$17.24 \pm 0.04$	$15.01 \pm 0.03$
<b>7a</b>	$31.58 \pm 0.07$	$17.99 \pm 0.04$	$19.77 \pm 0.04$	$17.27 \pm 0.04$
<b>7b</b>	$31.90 \pm 0.07$	$18.17 \pm 0.04$	$19.96 \pm 0.04$	$17.44 \pm 0.04$
ACA	$69.11 \pm 0.15$	—		
DIC			$49.33 \pm 0.11$	$41.88 \pm 0.09$

<sup>a</sup> Denotes the most effective compound, values were calculated from three replicates and expressed as mean  $\pm$  SE; ACA = acarbose; DIC = diclofenac sodium.



revealed that the four isatin-based Schiff bases **3b** ( $\alpha$ -amylase inhibition =  $54.76 \pm 0.12\%$ ), **5a** ( $\alpha$ -amylase inhibition =  $57.64 \pm 0.13\%$ ), **5b** ( $\alpha$ -amylase inhibition =  $55.96 \pm 0.12\%$ ), and **5c** ( $\alpha$ -amylase inhibition =  $56.52 \pm 0.12\%$ ) had anti-diabetic activities nearly close to the acarbose (standard reference), and the order of activity can be represented as **5a** > **5c** > **5b** > **3b**.

Modification of benzylidene derivative in compounds **2a** and **2b** by introducing secondary amine to form Schiff base containing amine moiety doesn't improve the activity. Furthermore, our work planned to study the effect of 5-azo-aryl-salicylamide-Schiff base derivatives **3a-d** on inhibition of  $\alpha$ -amylase and the result demonstrated that the presence of this moiety was affected directly by position and different substituent on azo-aryl group. Additionally, these derivatives showed good to potent inhibition percentages with values ranging between ( $\% = 31.33 \pm 0.07$  to  $54.76 \pm 0.12$ ). In addition, the introduction of a high electronegative atom as fluoro observed the best inhibition among these derivatives ( $\alpha$ -amylase inhibition =  $54.76 \pm 0.12\%$ ) with an inhibition percentage nearly of 79.23% compared to acarbose. Considering the *bis*-Schiff base **7a** and **7b**, it was noticed that the amylase percentage decreased, and that illustrated that repeated the isatin core as another heterocyclic core causes a decrease in the activity.

**2.2.3. Anti-Alzheimer's activity (acetylcholinesterase (AChE) enzyme inhibition).** Alzheimer's disease is a chronic neurodegenerative disease. For medicinal therapy, acetylcholinesterase inhibitors are used. Hence, in the USA, the only approved drug for Alzheimer's disease therapy is an acetylcholinesterase inhibitor which has proper effectiveness.<sup>52</sup> The anti-Alzheimer activity of isatin-based Schiff bases **2a**, **2b**, **3a-d**, **4**, **5a-c**, **6**, **7a**, and **7b** was assessed by determining the acetylcholinesterase (AChE) enzyme inhibition percentage,<sup>53</sup> and the results were listed in Table 2 and Fig. 3.

Generally, the inhibition percentage values toward the acetylcholinesterase for the designed isatin-Schiff bases 2–7 were determined and ranged from  $15.75 \pm 0.03$  to  $36.38 \pm 0.08\%$ . More importantly, four derivatives **3b**, **5a**, **5b**, and **5c**

revealed the highest inhibitory percentage on the acetylcholinesterase enzyme with values equal to  $34.56 \pm 0.08$ ,  $36.38 \pm 0.08$ ,  $35.32 \pm 0.08$ , and  $35.68 \pm 0.08\%$ , respectively. Interestingly, three of the four derivatives contain the same structure pattern with (1-phenyl-1*H*-pyrazol-4-yl) as a bioactive core side by side with 3-hydrazonoindoline pharmacophore with the new methylic group ( $\text{CH}=\text{N}$ ). Moreover, the values of inhibition to other derivatives **2a**, **2b**, **3a**, **3c**, **3d**, **4**, **6**, **7a**, and **7b** showed inhibition values ranging from  $15.75 \pm 0.03$  to  $19.61 \pm 0.04\%$ , indicating a narrow range between them.

**2.2.4. Anti-arthritis activity (proteinase denaturation and proteinase enzymes inhibition).** Arthritis is characterized by inflammation, which is one of its most important symptoms.<sup>54</sup> Proteinase denaturation and proteinase enzyme are the key features and indexes for the occurrence of inflammatory diseases, including arthritis.<sup>55</sup> Consequently, the ability of tested compounds to inhibit proteinase denaturation and proteinase enzymes refers to the apparent potential for anti-inflammatory activity.<sup>56,57</sup> An important aspect of protein denaturation is the modification of forces that stabilize proteins essential for their structure and function, such as disulfide bridges, ionic interactions, electrostatic forces, and hydrogen bonds. Additionally, anti-inflammatory drugs inhibit protein denaturation in dose-dependent ways.<sup>58</sup>

The anti-arthritis activity of the newly designed isatin-based Schiff bases derivatives **2a**, **2b**, **3a-d**, **4**, **5a-c**, **6**, **7a**, and **7b** was evaluated by determining the inhibition percentage of proteinase denaturation and proteinase enzyme. Firstly, the newly designed isatin-based Schiff bases showed proteinase denaturation inhibition (PDI) values ranging between ( $17.24 \pm 0.04$  to  $39.59 \pm 0.09\%$ ) and proteinase inhibition (PI) enzyme ( $15.01 \pm 0.03$  to  $36.39 \pm 0.08\%$ ) when compared with reference standard drug diclofenac sodium (proteinase denaturation  $\% = 49.33 \pm 0.11$  and proteinase inhibition  $\% = 41.88 \pm 0.09$ ) as represented in Table 2.

The present study observed the maximum percentage of proteinase denaturation inhibition (PDI) and proteinase

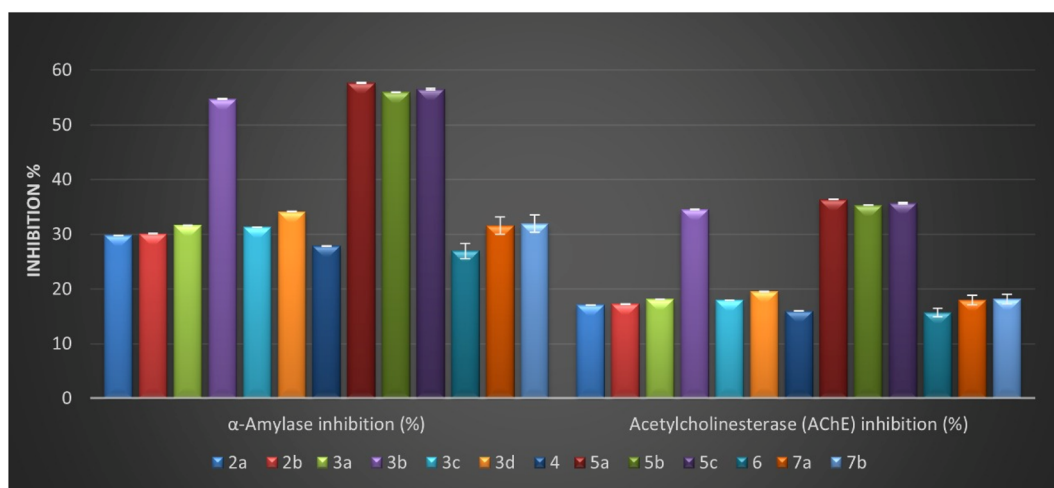


Fig. 3 *In vitro* anti-diabetic activity represented as  $\alpha$ -amylase inhibition (%) and anti-Alzheimer's activity represented as acetylcholinesterase (AChE) inhibition (%) of the newly designed derivatives 2–7.





inhibition (PI) by four Schiff bases **3b**, **5a**, **5b**, and **5c**. These derivatives revealed proteinase denaturation and proteinase inhibition in the range from  $37.61 \pm 0.08$  to  $39.59 \pm 0.09\%$  and from  $34.57 \pm 0.08$  to  $36.39 \pm 0.08\%$ , respectively, and close to the diclofenac sodium PDI =  $49.33 \pm 0.11\%$  and PI =  $41.88 \pm 0.09\%$  (Fig. 4 and Table 2). These good inhibitory activities can be referred to the presence of pyrazole moiety side by side with indolin-2-one in compounds **5a–c** that causes a diminution in protein denaturation and proteinase inhibitory activity and an increase in enhanced protection. Moreover, it was observed that the lowest anti-arthritis activity was determined by isatin Schiff base **6** with 1-phenyl-1*H*-pyrazole containing the benzo[*b*]furan group as a substituent in position two of the pyrazole motif. Compound **6** exhibited proteinase denaturation inhibition (PDI =  $17.24 \pm 0.04\%$ ) and proteinase inhibition (PI =  $15.01 \pm 0.03\%$ ) and this decrease in anti-arthritis activity may be related to the presence of a benzofuran group.

Furthermore, the *bis*-indolin-2-one derivatives **7a** and **7b** demonstrated low inhibitory activity against the proteinase denaturation inhibition (PDI =  $19.77 \pm 0.04$  and  $19.96 \pm 0.04\%$ ) and proteinase inhibition (PI =  $17.27 \pm 0.04$  and  $17.44 \pm 0.04\%$ ), respectively. In addition, compounds **2a** and **2b** that contain a hydrazone group with 4-(piperidin-1-yl or morpholin-1-yl)benzylidene moiety exhibited very close inhibitory activity to *bis*-indolin-2-one derivatives **7a** and **7b** with proteinase denaturation inhibition (PDI =  $19.23 \pm 0.04$  and  $19.40 \pm 0.04\%$ ) and proteinase inhibition (PI =  $17.03 \pm 0.04$  and  $17.19 \pm 0.04\%$ ), respectively.

Finally, it can be concluded that the newly developed isatin-based Schiff bases 2–7 reduce protein denaturation and proteinase inhibition, resulting in an anti-arthritis activity. In addition, among the synthesized derivatives, four Schiff bases **3b**, **5a**, **5b**, and **5c** displayed good inhibitory activity ranging between (76.2–80.25%) and (82.5–86.89%) compared to diclofenac.

As depicted in Table S1 (ESI file<sup>†</sup>), it was noticed that IRP, TAC, the scavenging activity against ABTs, the inhibitory effect

against  $\alpha$ -amylase and ACE in addition to the anti-arthritis activity are positively correlated with each other and negatively correlated with the concentration required to inhibit 50% of DPPH radicals ( $IC_{50}$ ). When these biological activities increase, the concentration required to inhibit 50% of the DPPH radical decreases.

**2.2.5. Structure–activity relationship (SAR) analysis.** The structure–activity relationship analysis revealed that the formation of a new azomethine group ( $CH=N$ ) to 3-hydrazonoindolin-2-one (**1**) improved biological evaluation Fig. 5. The SAR analysis based on the pharmacophore group introduced in the side chain of the main core can be illustrated as follows:

[I] Introducing the benzylidene derivative with morpholinyl or piperidinyl moiety exhibited moderate activity with a slight difference between the two derivatives, and the morpholinyl moiety often exhibited slight potency, and that may be related to the presence of hetero atom oxygen.

[II] Looking at the series of isatin-azomethine-aryl azo derivatives **3a–d**, the formation of salicylamide derivatives showed moderate activity in general, and the most potent derivative among this series is **3b** which is linked to the fluorine atom. This activity may be due to the small size and highly electronegative of fluorine atom, which can improve pharmacokinetics and drug-likeness properties.<sup>59,60</sup>

[III] Introduction of a new heterocyclic to the azomethine group as 5-methyl furan-2-yl motif does not improve activity, and this can be illustrated by the electron may run and push in the furan core more than the azomethine group and an indole moiety due to high electronegativity of the oxygen atom than the nitrogen.

[IV] The activity of the three isatin-based Schiff bases **5a**, **5b**, and **5c** may be related to the presence of the pyrazole scaffold with various substitutions. Additionally, the isatin-based Schiff base **5a**, with different substituents on pyrazole moiety as 5-chloro-3-methyl exhibited the most potent compound, which

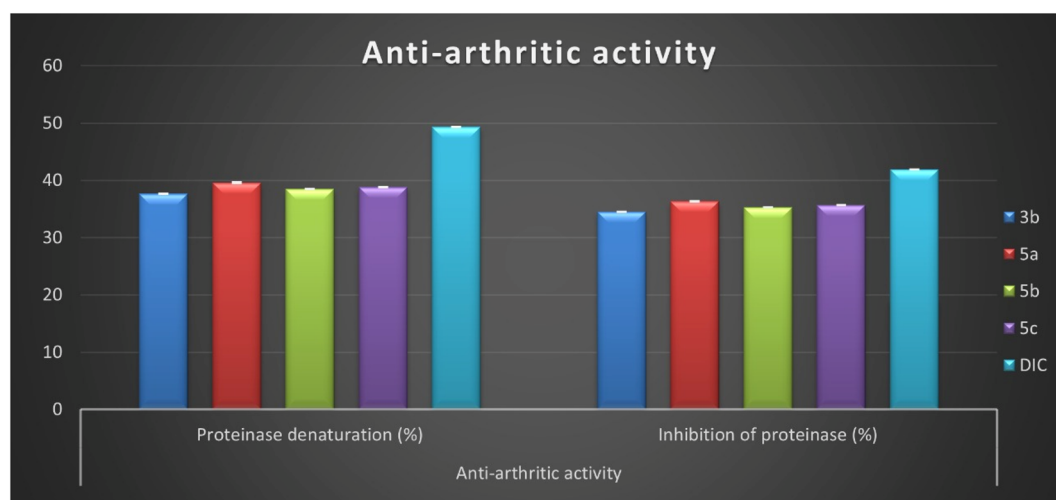


Fig. 4 *In vitro* inhibition percentage of anti-arthritis activity (proteinase denaturation and proteinase) of most active isatin derivatives **3b**, **5a**, **5b**, **5c**, and diclofenac sodium.



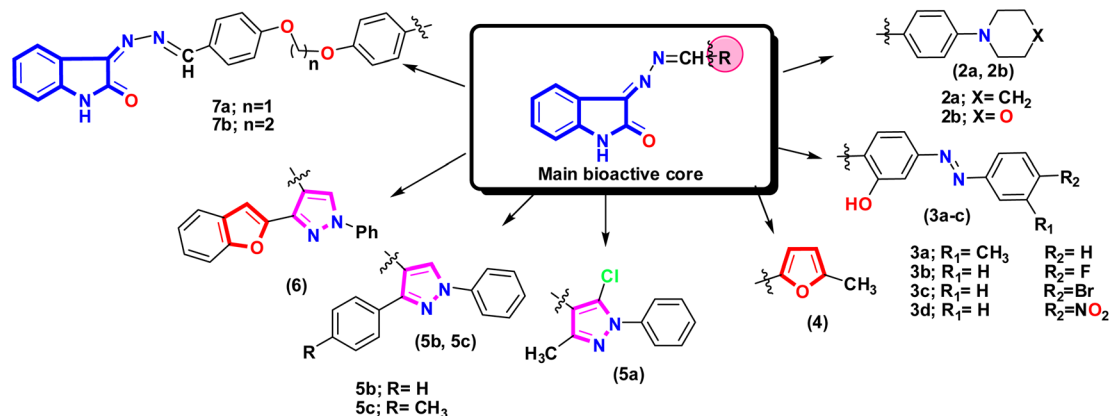


Fig. 5 Showed the different fragment that attached to 3-hydrazonoindolin-2-one (1) and formed new azomethine group with different pharmacophore that affect the activity.

may be due to increasing the hydrophobic properties in the pyrazole ring.<sup>61</sup>

[V] The two isatin-based Schiff bases **5b** and **5c** showed almost the same activities where the isatin-based Schiff base **5b** linked with the phenyl ring at C3 of the pyrazole moiety while derivative **5c** linked with the 4-methylphenyl ring at the same position (C3 of the pyrazole moiety) indicating that the methyl group in this position doesn't affect the activity. Additionally, replacing this aryl group with heteroatom-containing bicyclic moiety (benzofuran) at C-3 resulted in weaker activity.

[VI] It was observed that the incorporation of *bis*-formyl derivatives to 3-hydrazonoindolin-2-one (1) to form a *bis*-Schiff base with a dioxo-linker by introducing more lipophilic group (phenyl group) doesn't enhance the activity.

Finally, it can be concluded that the four compounds **3b**, **5a**, **5b**, and **5c** have high antioxidant, anti-diabetes, anti-Alzheimer's, and anti-arthritis activities. This result agrees with the result of Russo and co-workers, which state the relationship and well correlation between the biological activities of the compounds. Additionally, it was reported that the antioxidant activity improves and enhances some activities such as anti-diabetes, anti-Alzheimer's, and anti-arthritis.<sup>62</sup>

### 3. Computational studies

#### 3.1. Quantum chemical calculations

In medicinal chemistry, the density functional theory (DFT) is most commonly used in quantum chemical studies to confirm the structural features essential for biological activity.<sup>63,64</sup> Additionally, it was used widely because of its low cost, satisfactory performance, and understanding of molecules' behavior in the reactions.<sup>65,66</sup> In this work, the structure of the most active Schiff bases **3b**, **5a**, **5b**, and **5c** was constructed and optimized using the popular hybrid functional B3LYP with the double zeta basis set 6-31 g (d) as described previously.<sup>67-69</sup> The frontier molecular orbitals (FMO) are represented by the highest occupied orbital (HOMO) and lowest occupied orbital (LUMO), and, therefore, the difference between HOMO and LUMO defined as energy band gap and these descriptors are important to evaluate

the stability of compounds and intermolecular interaction in the drug-receptor binding system.<sup>70</sup>

As represented in Fig. 6, the salicylamide derivative **3b** showed that the HOMO orbital and LUMO were localized overall molecule. However, the HOMO orbital is condensed over the isatin nucleus and salicylamide-azo group with  $E_{\text{HOMO}} = -5.76$  eV and  $E_{\text{LUMO}} = -2.88$  eV. Similarly, compounds **5a-c** revealed that the HOMO orbitals are localized over all the molecules. At the same time, LUMO orbitals are distributed over all molecules except *N*-phenyl and chlorine atom attached to pyrazole (**5a**), two phenyl rings attached to pyrazole core (**5b**), and phenyl and tolyl bounded to pyrazole derivative (**5c**). Additionally, it was found that the hydrazone group ( $-\text{C}=\text{N}-\text{N}=\text{C}-$ ) contributed to both HOMO and LUMO orbitals. Moreover, compound **3b** exhibited the lowest energy band gap  $\Delta E = 2.88$  eV, while the other pyrazole derivatives **5a**, **5b**, and **5c** showed very close energy band gaps with values  $\Delta E = 3.42$ , 3.38, and 3.36 eV, respectively. Notably, the most active compound **5a** showed the lowest total energy with a value of  $E_{\text{Total}} = -1541.58$  Hartree compared to **5b** ( $E_{\text{Total}} = -1273.73$  Hartree), **5c** ( $E_{\text{Total}} = -1313.04$  Hartree), and salicylamide derivative **3b** ( $E_{\text{Total}} = -1332.63$  Hartree), and therefore, compound **5a** is the most stable and least reactive and these results may illustrate the potency of biological activity (Table S2, ESI file†).

The molecular electrostatic potential (MEP Maps) is an important tool that used to recognize the reactive sites in a molecule by determine the positive and negative regions through the molecules. These regions help to form different types of interaction as hydrogen bonds, arene-arene " $\pi-\pi$ ", arene-cation " $\pi$ -cation", and hydrophobic interactions inside the active site of pocket in the biological target.

The MEP maps diagram represents various electrostatic potentials on a molecule with different colors. Additionally, the electrostatic potential areas are colored based on their electrostatic potential and range from blue to red, the blue regions being the most positive, while the red regions being the most negative, and finally, the green regions being zero. The ascending order is expressed as the following: red > orange > yellow > green > blue. The red regions (negative charge) are



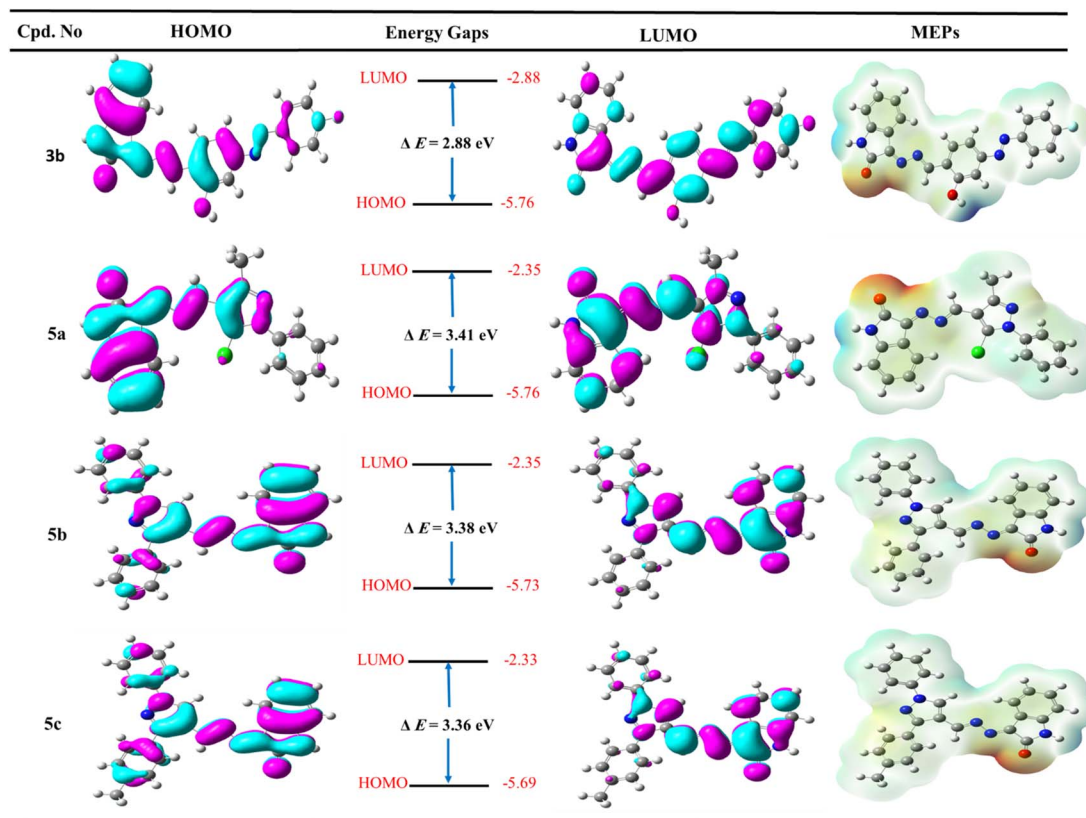


Fig. 6 The frontier molecular orbitals (HOMO and LUMO) and molecular electrostatic potential of the most active derivatives **3b**, **5a**, **5b**, and **5c**.

localized over the oxygen of isatin, nitrogen of hydrazone, oxygen of hydroxyl group and nitrogen of azo group in the salicylamide derivative **3b**, and nitrogen of pyrazole (mainly nitrogen number 2) at pyrazole-Schiff bases **5a–c**. Moreover, the blue color is mainly related to the hydrogen atom of NH of isatin and hydrogen of the hydroxyl group in the salicylamide derivative **3b**. The green color represented the neutral regions distributed over the whole molecule, especially the aromatic rings. These charged surface areas that represented as blue and red regions could form hydrogen bonds in molecular docking and, therefore, could bind to the active site and inhibit the target enzyme and appear the potency of the synthesized compound.

### 3.2. Molecular docking simulations

In developing and designing a new drug, molecular docking is a crucial approach used to predict how a synthesized compound is bound to a drug target protein and its affinity.<sup>71,72</sup> The docking simulation for the most active Schiff bases **3b**, **5a**, **5b**, and **5c** was evaluated inside the active sites of two proteins to determine the binding mode pattern, binding conformation, and different types of interaction of the active derivatives with the active site in enzymes. The human pancreatic  $\alpha$ -amylase complexed with co-crystallized ligand acarbose ( $\alpha$ -amylase PDB: 2QV4) was selected for anti-diabetic activity. Further, the recombinant human acetylcholinesterase (AChE) (PDB: 4EY7) was used for anti-Alzheimer's activity. The crystal structures of

these two proteins were downloaded from the protein data bank (<https://www.rcsb.org/>) and the active site was generated as described previously<sup>73</sup> using Molecular Operating Environment (MOE) software version 2009.10.

**3.2.1. Study the binding mode inside the active site of  $\alpha$ -amylase (PDB: 2QV4).** To evaluate and determine the different types of interaction that lead to potential inhibition of most active derivatives features, we inspected the crystal structure of human pancreatic  $\alpha$ -amylase complexed with co-crystallized ligand acarbose ( $\alpha$ -amylase PDB: 2QV4). The validation process exhibited binding energy  $S = -32.53 \text{ kcal mol}^{-1}$  and RMSD value of 1.13 Å through two hydrogen bonds sidechain acceptors (His201 and Arg195), four hydrogen bonds sidechain donor (Glu233, His299, and Asp300), and one hydrogen bond backbone donor (Ala106) (see ESI file†).

Interestingly, the Schiff base derivative **5a** revealed binding energy  $S = -22.09 \text{ kcal mol}^{-1}$  and interacted with the pocket *via* hydrogen bond acceptors with the side chain between the residue Arg195 and carbonyl of isatin with a distance of 2.67 Å and strength 17%. Besides, an arene–arene interaction was observed between Trp59 and phenyl of the *N*-phenyl pyrazole group. Moreover, the isatin bioactive core in compound **5b** could make two hydrogen bonds with the active site of pocket through NH of isatin with Glu240 (2.13 Å and 12%) and carbonyl of isatin derivative with Lys200 (2.00 Å and 32%), as well as arene–arene interaction between the phenyl of isatin and Tyr151 (Fig. 7, and full size figures represented in ESI file†).



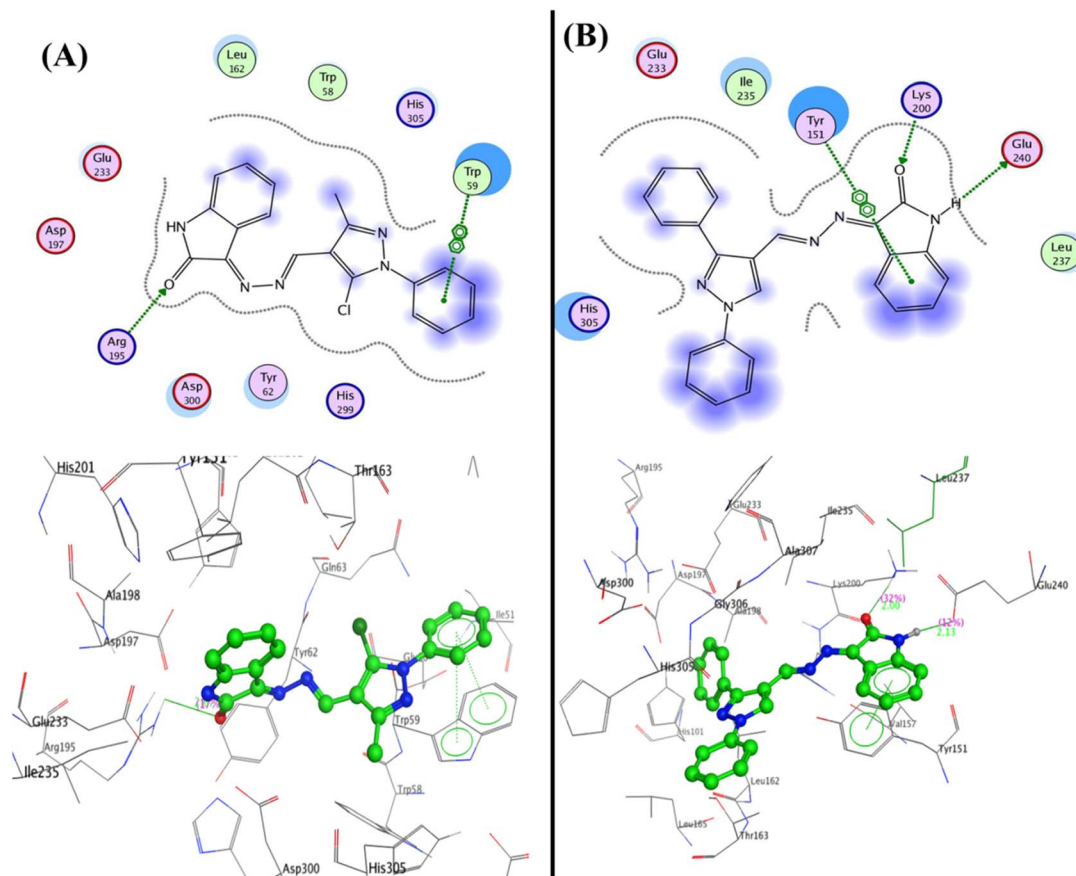


Fig. 7 2D and 3D structure of compounds (A) **5a** and (B) **5b** inside the active site of  $\alpha$ -amylase (PDB: 2QV4).

Furthermore, compound **5c** was able to interact with the residues in diverse sites in the pocket as Glu233 and formed a hydrogen bond sidechain donor with NH of isatin with a bond length of 2.17 Å and strength of 14%, moreover, it interacted with amino acids in the peripheral anionic site Trp59 and His101 through arene–arene “ $\pi$ – $\pi$ ” interactions with phenyl of *N*-phenyl of pyrazole and phenyl of isatin, respectively. Additionally, compound **3b** displayed two hydrogen bonds sidechain acceptors between the His201 and Lys200 with the hydroxyl group and carbonyl of isatin with bond lengths 2.18 Å (11%) and 1.93 Å (13%), respectively (Fig. 8).

**3.2.2. Study the binding mode inside the active site of acetylcholinesterase (AChE) (PDB: 4EY7).** The *in vitro* enzymatic inhibition showed that compounds **3b**, **5a**, **5b**, and **5c** are the most active derivatives with inhibition percentages ranging between  $34.56 \pm 0.08$ – $36.38 \pm 0.08\%$ , so the molecular docking simulation was used to identify, explain, and confirm the molecular mechanism of bioactive compounds with the active site of acetylcholinesterase (AChE) (PDB: 4EY7). Firstly, the validation process was performed by selection only one chain (B) and reproduced experimental poses with the RMSD of 0.714 Å with binding energy  $S = -32.42$  kcal mol<sup>−1</sup>. The co-crystallized ligand exhibited two arene–arene “ $\pi$ – $\pi$ ” interactions between the residues Trp86 and Trp286 with phenyl of *N*-benzylidene and phenyl of 1*H*-inden-1-one derivative,

respectively. Besides, the arene–cation “ $\pi$ –cation” interaction between the residue amino acid (Tyr337) and NH of piperidiny moiety and hydrophobic interaction that appears on the two methoxy groups (see ESI file† for all docking figures). Compound **5a** showed the highest inhibition percentage on acetylcholinesterase (AChE =  $36.38 \pm 0.08\%$ ) among the synthesized derivatives. Also, it displayed the highest binding energy  $S = -27.49$  kcal mol<sup>−1</sup> through one hydrogen bond side chain donor between the residue Glu202 and NH of isatin with bond length 2.20 and strength 19%. Additionally, the pyrazole core exhibited arene–arene “ $\pi$ – $\pi$ ” interaction with the amino acid Tyr341, while the *N*-phenyl of pyrazole produced another arene–arene “ $\pi$ – $\pi$ ” interaction with the residue Trp286 (Fig. 9).

Furthermore, the compounds **5b** and **5c** demonstrated one type of interaction known as arene–arene interaction with three residues of amino acid, where compound **5b** presented binding energy  $S = -27.22$  kcal mol<sup>−1</sup> with four arene–arene interactions between the residues Tyr124 and Tyr341 with phenyl of isatin and the Trp286 with *N*-phenyl of pyrazole and pyrazole bioactive core. At the same time, compound **5c** showed binding energy  $S = -25.61$  kcal mol<sup>−1</sup> with the residues Trp286, Tyr337, and Tyr341 with NH of isatin, *N*-phenyl of pyrazole and pyrazole bioactive core, respectively. Additionally, the hydrophobic interaction was observed inside the





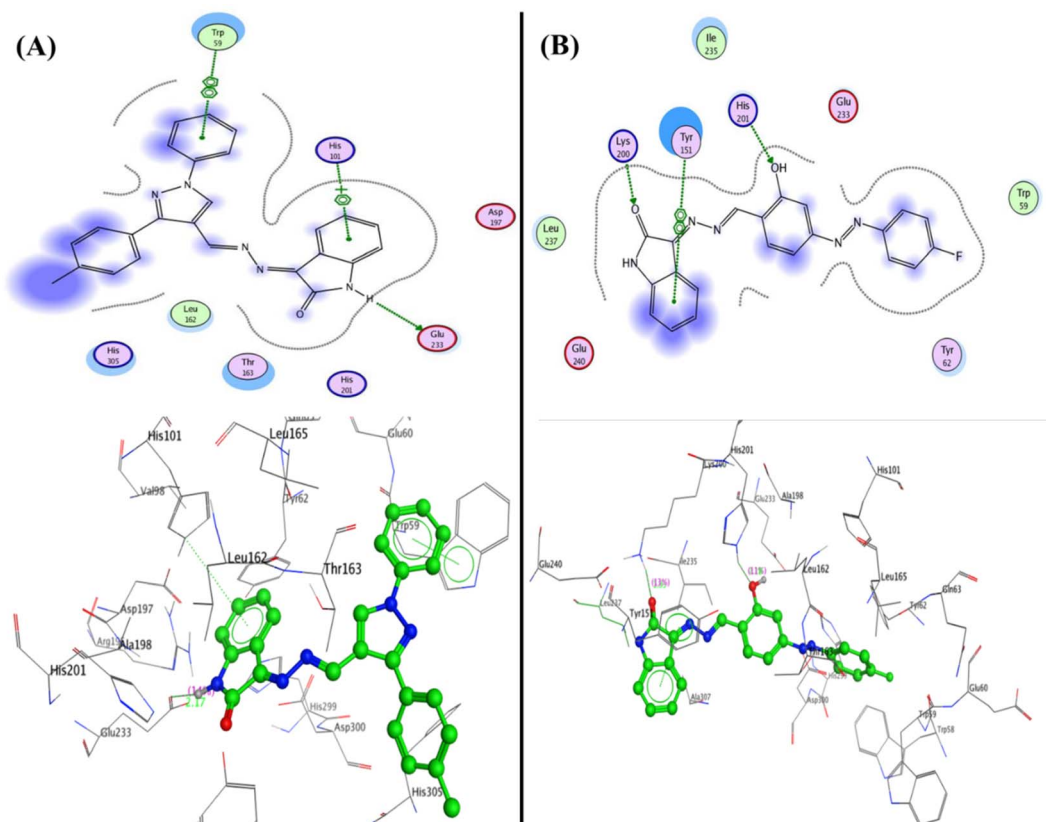


Fig. 8 2D and 3D structure of compounds (A) 5c and (B) 3b inside the active site of  $\alpha$ -amylase (PDB: 2QV4).

pocket with phenyl groups substituted on pyrazole, and phenyl of isatin moiety (Fig. 10). Finally, the salicylamide derivative 3b revealed the lowest binding energy  $S =$

$-24.66 \text{ kcal mol}^{-1}$  through one hydrogen bond backbone acceptor between the Phe295 with the hydroxyl group with a distance of 1.99 and strength of 27%, as well as one arene-

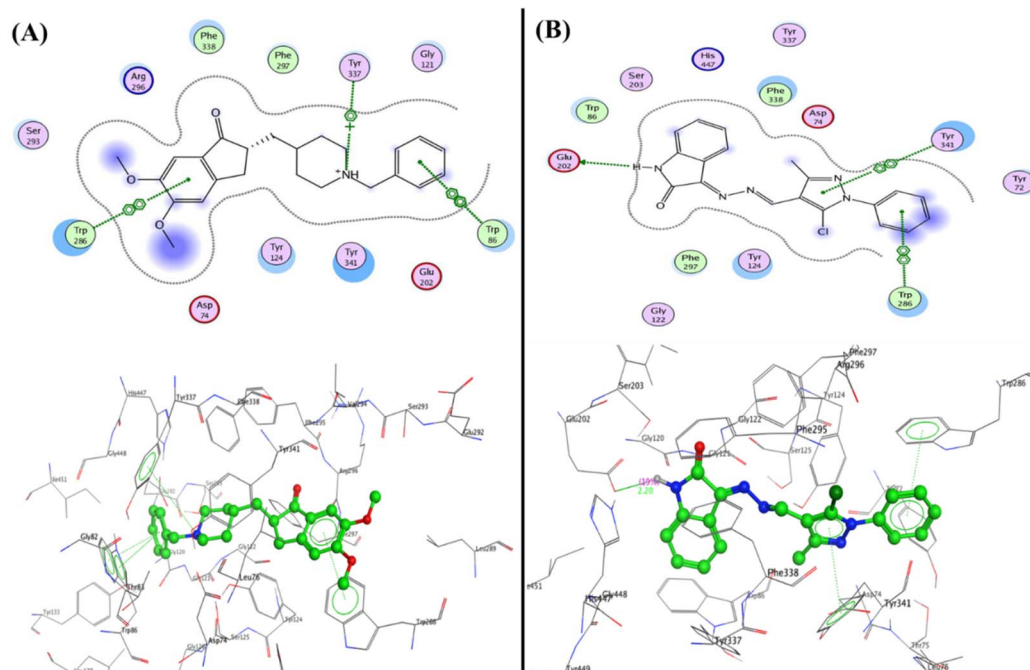
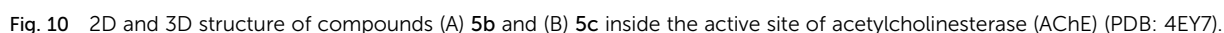


Fig. 9 2D and 3D structure of compounds (A) co-crystallized ligand and (B) 5a inside the active site of acetylcholinesterase (AChE) (PDB: 4EY7).





The selection of new drugs and formulations are based on the physicochemical properties, which include the molecular weight (MW), solubility, molar refractivity (MR), topological polar surface area (TPSA), and hydrogen-bonding capacities; therefore, the physicochemical properties of isatin-based Schiff bases **3b** and **5a–c** (Table 3) are the essential factors for finding new drug candidates and should be an agreement with the different rule-based filters (drug-likeness rules).<sup>76,77</sup>

The physicochemical properties and drug-likeness of isatin-based Schiff bases **3b** and **5a-c** were calculated using SwissADME website <http://www.swissadme.ch/index.php>.<sup>74</sup> While the drug-likeness scores were calculated using Molsoft LLC

Properties	3b	5a	5b	5c
Formula	C <sub>21</sub> H <sub>14</sub> FN <sub>5</sub> O <sub>2</sub>	C <sub>19</sub> H <sub>14</sub> ClN <sub>5</sub> O	C <sub>24</sub> H <sub>17</sub> N <sub>5</sub> O	C <sub>25</sub> H <sub>19</sub> N <sub>5</sub> O
Molecular weight (MW)	387.37	363.80	391.42	405.45
Num. Heavy atoms (atoms)	29	26	30	31
Num. aromatic heavy atoms (arom-atoms)	18	17	23	23
Fraction Csp <sup>3</sup>	0.00	0.05	0.00	0.04
Num. Rotatable bonds (R-bonds)	4	3	4	4
Num. H-bond acceptors (H-acc)	7	4	4	4
Num. H-bond donors (H-don)	2	1	1	1
Molar refractivity (MR)	111	105.5	120.96	125.92
Topological polar surface area (TPSA)	98.77	71.64	71.64	71.64
M log P (solubility)	2.48	2.48	2.90	3.11
W log P (solubility)	4.57	3.04	3.74	4.05
X log P (solubility)	4.15	4.15	4.26	4.62
Lipinski filter violations	0	0	0	0
Ghose filter violations	0	0	0	0
Veber (GSK) filter violations	0	0	0	0
Egan (pharmacia) filter violations	0	0	0	0
Drug-likeness model score	−0.14	0.05	−0.05	0.31

There are some drug-likeness rules<sup>78</sup> which can describe as (i) Lipinski's rule ( $MW \leq 500$ ;  $M \log P \leq 5$ ;  $H\text{-acc} \leq 10$ ;  $H\text{-don} \leq 5$ ), (ii) Ghose's filter ( $160 \leq MW \leq 480$ ,  $-0.4 \leq W \log P \leq 5.6$ ,  $40 \leq MR \leq 130$ , and  $20 \leq \text{atoms} \leq 70$ ), (iii) Veber's filter ( $R\text{-bonds} \leq 10$ , and  $TPSA \leq 140$ ), and (iv) Egan's filter ( $W \log P \leq 5.88$ , and  $TPSA \leq 131.6$ ). Based on these rules, we found that the four isatin-based Schiff bases (**3b** and **5a–c**) agree with the four drug-likeness rules (Lipinski, Ghose, Veber, and Egan rules) and these derivatives are accepted as new drug candidates.

The drug-likeness model score analysis is based on the positive and negative values of the target compounds, where the compound is like a drug if the drug-likeness score is valued positively. In contrast, the compound is non-drug if the drug-likeness score is valued negatively.<sup>79</sup> Based on this rule, we found that (i) the two Schiff bases, isatin-azomethine-pyrazole derivatives **5a** and **5c**, showed drug-likeness scores equal to 0.05 and 0.31, respectively, and therefore considered drug-like. (ii) On the other hand, the other two compounds, isatin-azomethine-aryl azo derivative **3b**, and isatin-pyrazole based Schiff base **5b**, revealed negative drug-likeness scores equal to  $-0.14$  and  $-0.05$ , respectively, and consequently, these compounds were non-drug like (Fig. 11).

**3.3.2. Toxicity and metabolism prediction analysis.** The toxic properties of isatin-based Schiff bases **3b** and **5a–c** were calculated using ADMETlab 2.0 website <https://admetmesh.scbdd.com/service/evaluation/cal>.<sup>80</sup> At the same

time, the metabolism properties were computed using the pkCSM-pharmacokinetics website <https://biosig.lab.uq.edu.au/pkcsm/prediction>,<sup>81</sup> also the probability value (the range of zero to one) of the metabolism properties had been calculated from the ADMETlab 2.0 website. All the properties were summed in Table 4.

Human hepatotoxicity (H-HT) is essential to risk inspection for new drugs. The destruction and injury of the liver because of the drug's effects is a major patient safety concern, and the drug may be withdrawn from the market. The new target compounds are either non-toxic for the liver, H-HT negative, with a value of 0 to 0.3 (green), or toxic for the liver, H-HT positive, with two categories; the first is moderate toxicity with a predicted value of 0.3 to 0.7 (yellow) and the second is strong toxicity with a value from 0.7 to 1.0 (red). All isatin-based Schiff bases **3b** and **5a–c** were predicted as liver toxic (H-HT positive) from the strong toxicity with high hazard (red color, the degree from 0.951 to 0.975).

Carcinogenic substances have the ability to damage the genome; as a result, they have serious effects on human health. Some drugs are withdrawn from the market when they are proven to be carcinogenic. The target compounds are marked as non-carcinogens with a predicted value of zero to 0.3 (green), moderately carcinogens with a predicted value of 0.3 to 0.7 (yellow) or strong carcinogens with a predicted value from 0.7 to 1.0 (red). Hence, compound **3b** is labeled a strong carcinogen

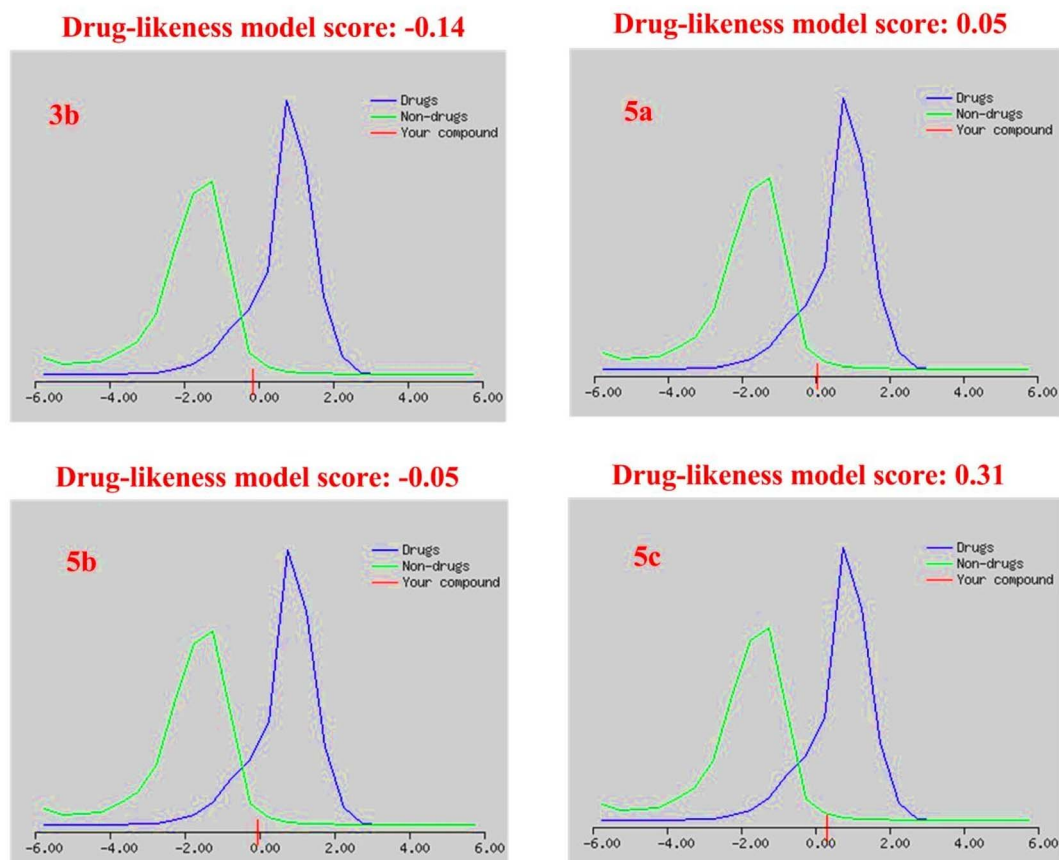


Fig. 11 The drug-likeness model scores of the isatin-based Schiff bases **3b** and **5a–c**.

Table 4 The toxicity and metabolism prediction of isatin-based Schiff bases **3b** and **5a–c**

Properties	<b>3b</b>	<b>5a</b>	<b>5b</b>	<b>5c</b>
<b>Toxicity</b>				
Human hepatotoxicity (H-HT)	0.974/●	0.975/●	0.951/●	0.958/●
Carcinogens	0.910/●	0.597/●	0.576/●	0.616/●
AMES test	0.969/●	0.754/●	0.447/●	0.558/●
Skin sensitization (SS)	0.600/●	0.650/●	0.173/●	0.102/●
Eye irritation (EI)	0.630/●	0.479/●	0.500/●	0.408/●
Eye corrosion (EC)	0.003/●	0.008/●	0.003/●	0.003/●
<b>Metabolism</b>				
CYP1A2 inhibitor	Yes/0.730	Yes/0.892	Yes/0.895	Yes/0.702
CYP2C19 inhibitor	Yes/0.578	Yes/0.521	Yes/0.840	Yes/0.777
CYP2C9 inhibitor	Yes/0.542	Yes/0.583	Yes/0.885	Yes/0.920
CYP2D6 inhibitor	No/0.022	No/0.011	No/0.020	No/0.022
CYP3A4 inhibitor	Yes/0.277	Yes/0.202	Yes/0.272	Yes/0.450

and exhibited a high predicted value of 0.910. At the same time, the three derivatives **5a**, **5b**, and **5c** are characterized as moderate carcinogens with a predicted value of 0.597, 0.576, and 0.616, respectively.

Furthermore, the Ames test for mutagenicity is used for testing the compound's mutagenicity, where the mutagenic has a close relationship with carcinogenicity. A target compound is considered strongly mutagenic when it has a predicted value of 0.7 to 1.0 (red) but considered a medium mutagenic when it has a predicted value of 0.3 to 0.7 (yellow) and considered a non-mutagenic when it has a predicted value of 0 to 0.3 (green). The compounds **3b** and **5a** are considered strongly mutagenic, but the compounds **5b** and **5c** are mutagenic from the medium degree. Additionally, evaluating the skin sensitization (SS), eye irritation (EI), and eye corrosion (EC) of substances is a necessary part of risk assessment. The target substances were divided into non-sensitizer/non-irritants/non-corrosive substances (value 0–0.3, green) or sensitizer/irritants/corrosive substances (high-risk substances with value 0.7–1.0 shown red color or medium substances risk with value 0.3–0.7 shown yellow color). The two Schiff bases **3b** and **5a** are skin sensitizers, but the other compounds **5b** and **5c** are non-sensitizers with values of 0.173 and 0.102, respectively. All isatin-based Schiff bases **3b** and **5a–c** were predicted as eye irritants (medium risk) and are predicted as eye non-corrosive substances.

Nowadays, the metabolism prediction model had concentrated on the interaction between the target compounds with cytochromes P450 monooxygenase enzymes (CYP1A2, CYP2C19, CYP2C9, CYP2D6, CYP3A4) which catalyze the phase 1 metabolism of pharmaceuticals and concentrated in the liver. The inhibition of cytochromes enzymes is one of the principal mechanisms which cause pharmacokinetic drug–drug interactions.<sup>82,83</sup> Table 4 demonstrates that all isatin-based Schiff bases **3b** and **5a–c** were predicted as inhibitors of the four enzymes (namely: CYP1A2, CYP2C19, CYP2C9, and CYP3A4) with the probability value range from 0.202 to 0.920. Also, predicted non-inhibition of the CYP2D6 enzyme of isatin-based Schiff bases **3b** and **5a–c** with a probability value ranging from 0.011 to 0.020.

**3.3.3. Absorption and distribution.** The absorption and distribution properties of isatin-based Schiff bases **3b** and **5a–c** were calculated using ADMETlab 2.0 website <https://admetmesh.scbdd.com/service/evaluation/cal>.<sup>84</sup> All the properties were summed in Table 5.

The new drug must pass *via* intestinal cell membranes before it reaches systemic circulation. To evaluate drug permeability, we utilized the human colon adenocarcinoma cell lines (Caco-2). Accordingly, Caco-2 cell permeability has been an important index for the new drug. A target compound is considered to fit proper Caco-2 permeability when it has a predicted value  $> -5.15 \log \text{ cm s}^{-1}$  (green). Based on the rule of Caco-2 permeability, we found that the four isatin-based Schiff bases (**3b** and **5a–c**) have a fit proper Caco-2 permeability with a range of  $-4.699$  to  $-4.827 \log \text{ cm s}^{-1}$ . The apparent permeability coefficient ( $P_{\text{app}}$ ) is used for estimating the uptake efficiency of target compounds in the body. Hence, the development of the Madin–Darby Canine Kidney cells (MDCK) for employing it as a model for permeability screening. Also, for evaluating the effect of the blood–brain barrier (BBB), we used  $P_{\text{app}}$  values of MDCK cell lines. A target compound is considered to have a high passive MDCK permeability when a  $P_{\text{app}}$  is more than  $20 \times 10^{-6} \text{ cm s}^{-1}$  (green). Table 5 illustrates that the target compounds **3b** and **5a–c** have a high passive MDCK permeability of more than  $20 \times 10^{-6} \text{ cm s}^{-1}$  in a range from  $1.4 \times 10^{-5}$  to  $2.1 \times 10^{-5} \text{ cm s}^{-1}$ .

P-glycoprotein (P-gp), known as MDR1 or 2 ABCB1, is an efflux membrane transporter and is responsible for limiting cellular uptake. Furthermore, P-gp is one of the main barriers to delivering drugs properly. Thus, a suitable inhibitor or substrate will allow an increase in cellular uptake and predict the pharmacokinetics of drugs.<sup>85</sup> A target compound is considered a fit proper P-glycoprotein inhibitor or substrate when it has a predicted value of zero to 0.3: excellent (green); 0.3–0.7: medium (yellow); 0.7–1.0: poor (red). Accordingly, the two Schiff bases **3b** and **5a** are inhibitors for P-glycoprotein with values of 0.013 and 0.001, respectively. Schiff base **5b** is a moderate P-glycoprotein inhibitor, but **5c** is a non-inhibitor of P-glycoprotein. On the other hand, the four isatin-based Schiff



Table 5 The absorption and distribution properties prediction of isatin-based Schiff bases **3b** and **5a–c**

Properties	<b>3b</b>	<b>5a</b>	<b>5b</b>	<b>5c</b>
<b>Absorption</b>				
Caco-2 permeability ( $\log \text{ cm s}^{-1}$ )	−4.781/●	−4.699/●	−4.842/●	−4.827/●
MDCK permeability ( $\text{cm s}^{-1}$ )	$1.7 \times 10^{-5}$ /●	$2.1 \times 10^{-5}$ /●	$1.6 \times 10^{-5}$ /●	$1.4 \times 10^{-5}$ /●
P-glycoprotein-inhibitor	0.013/●	0.001/●	0.304/●	0.799/●
P-glycoprotein-substrate	0.017/●	0.003/●	0.001/●	0.001/●
<b>Distribution</b>				
Plasma protein binding (PPB, %)	100.3/●	98.68/●	100.6/●	100.8/●
Fraction unbound in plasma (FU, %)	1.268/●	2.537/●	1.423/●	1.586/●
Volume distribution (VD, $\text{L kg}^{-1}$ )	0.987/●	1.964/●	0.476/●	0.39/●

bases (**3b** and **5a–c**) are P-glycoprotein substrates with predicted values a range from 0.001 to 0.017.

The pharmacodynamic behavior of the drugs is affected by their plasma protein binding (PPB) and the fraction unbound in plasma (FU). In general, drugs in plasma exist in an equilibrium state, unbound, or bound to serum proteins. Thus, the distribution of the drugs through the binding with plasma protein is one of the most important evaluations of drugs. A target compound is considered to have proper plasma protein binding if it has a predicted value of PPB of less than 90% (excellent, green) and a predicted value of FU of more than or equal to 5% (excellent, green). On the other hand, the drugs with a high binding with plasma protein of more than 90% (poor, red), and a predicted value for FU less than 5%, may have a low therapeutic index and decreased efficiency of traverse through cellular membranes. Based on the above, the four isatin-based Schiff bases (**3b** and **5a–c**) have a high binding with plasma protein with predicted values of more than 90% (the range from 98.68% to 100.8%), also the predicted values of FU less than 5% (the range from 1.268% to 2.537%), and these compounds maybe have a low therapeutic index with slight efficiency in crossing the membranes.

The volume distribution (VD) is an important parameter to describe the *in vivo* distribution of the drug. Volume distribution (VD) is a theoretical concept that links the administered dose of the drug with the actual initial concentration presented in the circulation. If the target compound has a predicted value of volume distribution in the range of 0.04 to 20  $\text{L kg}^{-1}$  (green), thus this compound has a good volume distribution. Table 5 depicts that all the target isatin-based Schiff bases **3b** and **5a–c** have a suitable volume distribution ranging from 0.39 to 1.964  $\text{L kg}^{-1}$ .

## 4. Conclusion

In summary, based on a new technique “one drug-multiple targets” for discovering novel therapeutics, novel derivatives of isatin-based Schiff bases (**2a**, **2b**, **3a–d**, **4**, **5a–c**, **6**, **7a**, and **7b**) have been synthesized and were proved by physical and spectral analysis. The work was extended to evaluate multiple biological activities, such as antioxidant, anti-diabetic, anti-Alzheimer, and anti-arthritis activities *in vitro* of all isatin-based Schiff

bases. The *in vitro* biological studies revealed that compound **5a** possessed multiple-active and exhibited potency as an antioxidant, scavenging, anti-diabetic, and anti-Alzheimer among the four potent derivatives (**3a** and **5a–c**). Also, the order of the potency is **5a** > **5c** > **5b** > **3b**. Furthermore, the computational studies of the most active Schiff bases **3b**, **5a**, **5b**, and **5c** were performed, and the quantum chemical calculation revealed that the most active compound **5a** is the most stable and least reactive with the lowest total energy and a value of  $E_{\text{Total}} = -1541.58$  Hartree. The docking simulation for **5a** revealed binding energy  $S = -22.09$  and  $-27.49 \text{ kcal mol}^{-1}$  compared with  $S = -32.53 \text{ kcal mol}^{-1}$  for acarbose and  $S = -32.42 \text{ kcal mol}^{-1}$  for donepezil inside the active sites of the two enzymes  $\alpha$ -amylase and acetylcholinesterase, respectively. Also, the drug-likeness prediction showed that the four active isatin-based Schiff bases (**3b** and **5a–c**) agree with the four drug-likeness rules (Lipinski, Ghose, Veber, and Egan rules) and these derivatives are accepted as new drug candidates, especially the two derivatives **5a** and **5c** that possess drug-likeness scores equal to 0.05 and 0.31, respectively, and therefore considered drug-like molecules. Finally, the *in silico* ADMET properties results of the isatin-based Schiff bases (**3b** and **5a–c**) indicate that (i) the Schiff bases (**3b** and **5a–c**) are inhibitors of CYP1A2, CYP2C19, CYP2C9, and CYP3A4 enzymes with the high probability value from 0.202 to 0.920, (ii) are non-inhibitors of the CYP2D6 enzyme with a probability value from 0.011 to 0.020, (iii) some Schiff bases possess low toxicity and other with moderate or high toxicity, (iv) the two Schiff bases **3b** and **5a** have high absorption properties, but almost all the Schiff bases (**3b** and **5a–c**) possess low distribution properties. From this contemporary manuscript, in the future, the four isatin-based Schiff bases **3b**, **5a**, **5b**, and **5c**, especially Schiff base **5a** will be utilized for the design of further structurally optimized derivatives based on the structure-activity relationship study with further biological evaluation for producing a novel drug with multiple targets “one drug-multiple targets”.

## 5. Materials and methods

### 5.1. Chemistry

All melting points were measured on a Gallenkamp melting point apparatus and are uncorrected. The IR spectra were





recorded (KBr disk) on a PerkinElmer 1650 FTIR instrument.  $^1\text{H}$ -NMR (500 MHz) and  $^{13}\text{C}$ -NMR (126 MHz) spectra were recorded on a JEOL spectrometer using  $\text{DMSO}-d_6$  as solvent and tetramethylsilane (TMS) as an internal standard. Chemical shifts ( $\delta$ -values) are reported in ppm. Elemental analyses were performed at the Micro Analytical Center, Cairo University, Egypt. Additionally, the progress of the reactions was monitored by thin-layer chromatography (TLC) using aluminum sheets coated with silica gel F<sub>254</sub> (Merck), viewing under a short-wavelength UV lamp effected detection. All evaporations were performed under reduced pressure at 40 °C.

Glacial acetic acid, *p*-fluoroaniline, *p*-nitroaniline, *m*-methylaniline, *p*-bromoaniline, ethanol, 5-methyl furan-2-carbaldehyde, *p*-fluorobenzaldehyde, *p*-hydroxybenzaldehyde, *o*-hydroxybenzaldehyde, and hydrochloric acid were of Fluka. Isatin and hydrazine hydrate were supplied by Aldrich.

## 5.2. General producer for the synthesis of isatin-based Schiff bases 2a, 2b, 3a–d, 4, 5a–c, 6, 7a, and 7b

A mixture of 3-hydrazino-isatin (**1**) (0.01 mol, 1.66 g) and the appropriate aldehydes (0.01 mol) {namely; 4-(piperidin-1-yl) benzaldehyde, 4-morpholinobenzaldehyde, 2-hydroxy-4-((3-methylphenyl)azo)benzaldehyde, 4-((4-fluorophenyl)azo)-2-hydroxybenzaldehyde, 4-((4-bromophenyl)azo)-2-hydroxybenzaldehyde, 2-hydroxy-4-((4-nitrophenyl)azo) benzaldehyde, 5-methylfuran-2-carbaldehyde, 5-chloro-3-methyl-1-phenyl-1*H*-pyrazole-4-carbaldehyde, 1, 3-diphenyl-1*H*-pyrazole-4-carbaldehyde, 1-phenyl-3-(4-methylphenyl)-1*H*-pyrazole-4-carbaldehyde, 3-(benzofuran-2-yl)-1-phenyl-1*H*-pyrazole-4-carbaldehyde, 4,4'-methylenebis(oxy)dibenzaldehyde, and 4,4'-(ethane-1, 2-diylbis(oxy))dibenzaldehyde} with a catalytic amount of glacial acetic acid (0.0087 mol, 0.5 mL) in absolute ethanol (25 mL) was refluxed for four hours and then left to cool. The solid product was filtered off, dried, and finally recrystallized from ethanol to afford Schiff bases **2a**, **2b**, **3a–d**, **4**, **5a–c**, **6**, **7a**, and **7b**.

**5.2.1. 3-((4-(Piperidin-1-yl)benzylidene)hydrazono)indolin-2-one (2a).** Red crystals, M.p.: 244–246 °C, yield (80%); IR (KBr)  $\nu_{\text{max}}/\text{cm}^{-1}$  3171 (NH), 1723 (C=O), 1605 (C=N), 1511 (C=C);  $^1\text{H}$  NMR ( $\text{DMSO}-d_6$ , 500 MHz,  $\delta$  ppm): 1.55 (s, 6H, 3CH<sub>2</sub>, piperidine moiety), 3.35 (s, 4H, 2CH<sub>2</sub>, piperidine moiety), 6.86 (d, 1H,  $J$  = 8.0 Hz, aromatic-H), 6.99 (d, 2H,  $J$  = 8.5 Hz, aromatic-H), 7.03 (t, 1H,  $J$  = 7.5 Hz, aromatic-H), 7.34 (t, 1H,  $J$  = 7.5 Hz, aromatic-H), 7.78 (d, 2H,  $J$  = 9.0 Hz, aromatic-H), 8.16 (d, 1H,  $J$  = 7.5 Hz, aromatic-H), 8.57 (s, 1H, –CH=N–, azomethine), 10.74 (s, 1H, NH-isatin exchangeable with D<sub>2</sub>O);  $^{13}\text{C}$  NMR ( $\text{DMSO}-d_6$ , 126 MHz,  $\delta$  ppm): 24.49, 25.45, 48.37 (5C, piperidine moiety), 111.12, 114.47, 114.85, 117.59, 122.26, 122.68, 129.29, 131.75, 133.46, 145.06, 150.77, 154.14, 164.75 (14C, 13C of aromatic + 1C of azomethine –N=CH–), 165.66 (1C, C=O); anal. calcd. (%) for C<sub>20</sub>H<sub>20</sub>N<sub>4</sub>O (332.40): C, 72.27; H, 6.06; N, 16.86. Found: C, 72.19; H, 6.10; N, 16.79%.

**5.2.2. 3-((4-Morpholinobenzylidene)hydrazono)indolin-2-one (2b).** Orange crystals, M.p.: 275–277 °C, yield (82%); IR (KBr)  $\nu_{\text{max}}/\text{cm}^{-1}$  3193 (NH), 1725 (C=O), 1611 (C=N), 1521 (C=C);  $^1\text{H}$  NMR ( $\text{DMSO}-d_6$ , 500 MHz,  $\delta$  ppm) 3.27–3.29 (m, 4H,

2CH<sub>2</sub>, morpholine moiety), 3.71 (s, 4H, 2CH<sub>2</sub>, morpholine moiety), 6.86 (d, 1H,  $J$  = 6.5 Hz, aromatic-H), 7.00 (t, 2H,  $J$  = 7.75 Hz, aromatic-H), 7.05 (d, 2H,  $J$  = 9.0 Hz, aromatic-H), 7.34 (t, 1H,  $J$  = 7.75 Hz, aromatic-H), 7.82 (d, 2H,  $J$  = 9.0 Hz, aromatic-H), 8.11 (d, 1H,  $J$  = 7.5 Hz, aromatic-H), 8.58 (s, 1H, –CH=N–, azomethine), 10.75 (s, 1H, NH-isatin exchangeable with D<sub>2</sub>O);  $^{13}\text{C}$  NMR ( $\text{DMSO}-d_6$ , 126 MHz,  $\delta$  ppm) 47.42, 66.40 (4C, morpholine moiety), 111.18, 114.54, 117.47, 122.75, 123.64, 129.34, 131.46, 133.65, 145.17, 150.98, 154.26, 164.17 (14C, 13C of aromatic + 1C of azomethine –N=CH–), 165.54 (1C, C=O); anal. calcd. (%) for C<sub>19</sub>H<sub>18</sub>N<sub>4</sub>O<sub>2</sub> (334.37): C, 68.25; H, 5.43; N, 16.76. Found: C, 68.19; H, 5.50; N, 16.82%.

**5.2.3. 3-((2-Hydroxy-4-((3-methylphenyl)azo)benzylidene)hydrazono)indolin-2-one (3a).** Orange crystals, M.p.: 283–285 °C, yield (88%); IR (KBr)  $\nu_{\text{max}}/\text{cm}^{-1}$  3433 (OH), 3157 (NH), 1716 (C=O), 1621 (C=N), 1536 (C=C);  $^1\text{H}$  NMR ( $\text{DMSO}-d_6$ , 500 MHz,  $\delta$  ppm) 2.42 (s, 3H, CH<sub>3</sub>), 6.92 (t, 1H,  $J$  = 5.8 Hz, aromatic-H), 7.08 (dd, 1H,  $J$  = 15.5, 7.8 Hz, aromatic-H), 7.20 (d, 1H,  $J$  = 10.0 Hz, aromatic-H), 7.37 (d, 1H,  $J$  = 6.5 Hz, aromatic-H), 7.44 (t, 1H,  $J$  = 8.0 Hz, aromatic-H), 7.49 (t, 1H,  $J$  = 6.5 Hz, aromatic-H), 7.70 (d, 2H,  $J$  = 8.0 Hz, aromatic-H), 7.95 (d, 1H,  $J$  = 7.0 Hz, aromatic-H), 8.01 (d, 1H,  $J$  = 8.5 Hz, aromatic-H), 8.50 (s, 1H, aromatic-H), 8.87 (s, 1H, –N=CH–), 10.91 (s, 1H, OH exchangeable with D<sub>2</sub>O), 11.47 (s, 1H, NH-isatin exchangeable with D<sub>2</sub>O);  $^{13}\text{C}$  NMR ( $\text{DMSO}-d_6$ , 126 MHz,  $\delta$  ppm) 21.41 (1C, CH<sub>3</sub>), 118.77, 120.40, 120.56, 122.39, 122.90, 123.47, 129.54, 130.02, 134.17, 139.46, 145.75, 151.06, 152.56, 157.93, 161.78 (20C, 19C of aromatic + 1C of azomethine –N=CH–), 165.07 (1C, C=O); anal. calcd. (%) for C<sub>22</sub>H<sub>17</sub>N<sub>5</sub>O<sub>2</sub> (383.40): C, 68.92; H, 4.47; N, 18.27. Found: C, 68.85; H, 4.51; N, 18.20%.

**5.2.4. 3-((4-((4-Fluorophenyl)azo)-2-hydroxybenzylidene)hydrazono)indolin-2-one (3b).** Orange crystals, M.p.: 261–263 °C, yield (85%). IR (KBr)  $\nu_{\text{max}}/\text{cm}^{-1}$  3440 (OH), 3194 (NH), 1715 (C=O), 1620 (C=N), 1535 (C=C);  $^1\text{H}$  NMR ( $\text{DMSO}-d_6$ , 500 MHz,  $\delta$  ppm) 6.91 (t, 1H,  $J$  = 8.0 Hz, aromatic-H), 7.05–7.10 (m, 1H, aromatic-H), 7.19 (dd, 1H,  $J$  = 9.5, 2.5 Hz, aromatic-H), 7.42 (d, 2H,  $J$  = 8.0 Hz, aromatic-H), 7.45 (d, 1H,  $J$  = 10.0 Hz, aromatic-H), 7.91–8.01 (m, 4H, aromatic-H), 8.50 (s, 1H, aromatic-H), 8.87 (s, 1H, –N=CH–, azomethine), 10.90 (s, 1H, OH exchangeable with D<sub>2</sub>O), 11.03 (s, 1H, NH-isatin exchangeable with D<sub>2</sub>O);  $^{13}\text{C}$  NMR ( $\text{DMSO}-d_6$ , 126 MHz,  $\delta$  ppm) 111.51, 116.75, 116.93, 118.26, 120.40, 122.84, 123.21, 124.50, 125.01, 125.09, 125.17, 127.67, 128.82, 129.74, 145.72, 149.23, 149.25, 151.14, 158.17, 161.91 (20C, 19C of aromatic + 1C of azomethine –N=CH–), 165.07 (1C, C=O); anal. calcd. (%) for C<sub>21</sub>H<sub>14</sub>FN<sub>5</sub>O<sub>2</sub> (387.37): C, 65.11; H, 3.64; N, 18.08. Found: C, 65.20; H, 3.58; N, 18.01%.

**5.2.5. 3-((4-((4-Bromophenyl)azo)-2-hydroxybenzylidene)hydrazono)indolin-2-one (3c).** Orange crystals, M.p.: 290–292 °C, yield (82%); IR (KBr)  $\nu_{\text{max}}/\text{cm}^{-1}$  3432 (OH), 3196 (NH), 1718 (C=O), 1618 (C=N), 1574 (C=C);  $^1\text{H}$  NMR ( $\text{DMSO}-d_6$ , 500 MHz,  $\delta$  ppm) 6.93 (d, 1H,  $J$  = 7.5 Hz, aromatic-H), 7.07 (t, 1H,  $J$  = 7.5 Hz, aromatic-H), 7.19 (d, 1H,  $J$  = 8.5 Hz, aromatic-H), 7.43 (t, 1H,  $J$  = 8.3 Hz, aromatic-H), 7.79 (d, 2H,  $J$  = 9.0 Hz, aromatic-H), 7.83 (d, 2H,  $J$  = 8.5 Hz, aromatic-H), 7.93 (d, 1H,  $J$  = 7.0 Hz, aromatic-H), 7.99–8.02 (m, 1H, aromatic-H), 8.33–8.51 (m, 1H, aromatic-H), 8.86 (s, 1H, –N=CH–, azomethine), 10.90 (s, 1H, OH exchangeable with D<sub>2</sub>O), 11.56 (s, 1H, NH-isatin





exchangeable with D<sub>2</sub>O); <sup>13</sup>C NMR (DMSO-*d*<sub>6</sub>, 126 MHz,  $\delta$  ppm) 111.54, 116.93, 118.35, 118.89, 120.51, 122.89, 124.64, 124.81, 127.84, 128.86, 133.02, 134.43, 145.63, 145.74, 151.11, 151.41, 157.84, 162.15 (20C, 19C of aromatic + 1C of azomethine -N=CH-), 165.06 (1C, C=O); MS (*m/z*, %): 450 (M + 2, 10.81), 448 (M<sup>+</sup>, 13.25), 219 (100); anal. calcd. (%) for C<sub>21</sub>H<sub>14</sub>BrN<sub>5</sub>O<sub>2</sub> (448.27): C, 56.27; H, 3.15; N, 15.62. Found: C, 56.20; H, 3.21; N, 15.56%.

**5.2.6. 3-((2-Hydroxy-4-((4-nitrophenyl)azo)benzylidene)hydrazono)indolin-2-one (3d).** Red crystals, M.p.: 279–281 °C, yield (86%); IR (KBr)  $\nu_{\text{max}}/\text{cm}^{-1}$  3429 (OH), 3200 (NH), 1726 (C=O), 1618 (C=N), 1516 (C=C); <sup>1</sup>H NMR (DMSO-*d*<sub>6</sub>, 500 MHz,  $\delta$  ppm) 6.85 (t, 1H, *J* = 7.5 Hz, aromatic-H), 7.04 (t, 1H, *J* = 7.5 Hz, aromatic-H), 7.15 (d, 1H, *J* = 9.0 Hz, aromatic-H), 7.40 (d, 1H, *J* = 8.5 Hz, aromatic-H), 7.59 (d, 1H, *J* = 7.5 Hz, aromatic-H), 7.89 (d, 1H, *J* = 8.0 Hz, aromatic-H), 8.01 (d, 2H, *J* = 9.0 Hz, aromatic-H), 8.34 (d, 2H, *J* = 7.5 Hz, aromatic-H), 8.50 (s, 1H, aromatic-H), 8.81 (s, 1H, -N=CH-, azomethine), 10.97 (s, 1H, OH exchangeable with D<sub>2</sub>O), 12.56 (s, 1H, NH-isatin exchangeable with D<sub>2</sub>O); <sup>13</sup>C NMR (DMSO-*d*<sub>6</sub>, 126 MHz,  $\delta$  ppm) 111.52, 116.88, 118.45, 120.66, 122.91, 123.74, 123.83, 125.30, 125.59, 128.20, 128.93, 134.46, 145.70, 148.57, 151.15, 155.75, 157.52, 162.96 (20C, 19C of aromatic + 1C of azomethine -N=CH-), 165.04 (1C, C=O); anal. calcd. (%) for C<sub>21</sub>H<sub>14</sub>N<sub>6</sub>O<sub>4</sub> (414.37): C, 60.87; H, 3.41; N, 20.28. Found: C, 60.80; H, 3.48; N, 20.34%.

**5.2.7. 3-(((5-Methylfuran-2-yl)methylene)hydrazono)indolin-2-one (4).** Orange crystals; M.p.: 160–162 °C; yield (84%); IR (KBr)  $\nu_{\text{max}}/\text{cm}^{-1}$  3203 (NH), 1729 (C=O), 1617 (C=N), 1536 (C=C); <sup>1</sup>H NMR (DMSO-*d*<sub>6</sub>, 500 MHz,  $\delta$  ppm) 2.38 (s, 3H, CH<sub>3</sub>), 6.50 (d, 1H, *J* = 3.7 Hz, furan H-4), 6.93 (d, 1H, *J* = 8.1 Hz, isatin), 7.08 (t, 1H, isatin), 7.30 (d, 1H, *J* = 3.7 Hz, furan H-3), 7.43 (t, 1H, isatin), 8.15 (d, 1H, *J* = 8.3 Hz, isatin), 8.53 (s, 1H, -CH=N-, azomethine), 10.87 (s, 1H, NH-isatin exchangeable with D<sub>2</sub>O); <sup>13</sup>C NMR (DMSO-*d*<sub>6</sub>, 126 MHz,  $\delta$  ppm) 13.74 (1C, CH<sub>3</sub>), 109.98, 110.61, 116.76, 121.63, 122.16, 128.93, 133.38, 144.71, 147.74, 151.09, 158.13, 163.36 (12C, 11C of aromatic + 1C of azomethine -N=CH-), 164.72 (1C, C=O); anal. calcd. (%) for C<sub>14</sub>H<sub>11</sub>N<sub>3</sub>O<sub>2</sub> (253.26): C, 66.40; H, 4.38; N, 16.59. Found: C, 66.45; H, 4.32; N, 16.64%.

**5.2.8. 3-(((3-Chloro-3-methyl-1-phenyl-1H-pyrazol-4-yl)methylene)hydrazono)indolin-2-one (5a).** Orange crystals; M.p.: 268–270 °C; yield (86%); IR (KBr)  $\nu_{\text{max}}/\text{cm}^{-1}$  3190 (NH), 1733 (C=O), 1622 (C=N), 1550 (C=C); <sup>1</sup>H NMR (DMSO-*d*<sub>6</sub>, 500 MHz,  $\delta$  ppm) 2.58 (s, 3H, CH<sub>3</sub>), 6.89 (d, 1H, *J* = 8.3 Hz, isatin), 7.03 (t, 1H, isatin), 7.39 (t, 1H, isatin), 7.52–7.65 (m, 5H, aromatic-H), 8.15 (d, 1H, *J* = 8.3 Hz, isatin), 8.65 (s, 1H, -CH=N-, azomethine), 10.85 (s, 1H, NH-isatin exchangeable with D<sub>2</sub>O). <sup>13</sup>C NMR (DMSO-*d*<sub>6</sub>, 126 MHz,  $\delta$  ppm) 14.76 (1C, CH<sub>3</sub>), 111.34, 113.27, 117.11, 122.77, 125.76, 128.86, 129.68, 129.91, 130.44, 134.18, 137.56, 145.50, 150.70, 151.45, 156.06 (17C, 16C of aromatic + 1C of azomethine -N=CH-), 165.34 (1C, C=O); MS (*m/z*, %): 365 (M + 2, 2.75), 363 (M<sup>+</sup>, 6.97), 77 (100); anal. calcd. (%) for C<sub>19</sub>H<sub>14</sub>ClN<sub>5</sub>O (363.80): C, 62.73; H, 3.88; N, 19.25. Found: C, 62.67; H, 3.94; N, 19.19%.

**5.2.9. 3-(((1,3-Diphenyl-1H-pyrazol-4-yl)methylene)hydrazono)indolin-2-one (5b).** Orange crystals; M.p.: 236–238 °C; yield (81%); IR (KBr)  $\nu_{\text{max}}/\text{cm}^{-1}$  3198 (NH), 1726 (C=O), 1613

(C=N), 1536 (C=C); <sup>1</sup>H NMR (DMSO-*d*<sub>6</sub>, 500 MHz,  $\delta$  ppm) 6.83 (d, 1H, *J* = 8.0 Hz, isatin), 6.90 (t, 1H, isatin), 7.34 (t, 1H, aromatic-H), 7.41 (t, 1H, isatin), 7.49–7.58 (m, 5H, aromatic-H), 7.74 (d, 2H, *J* = 8.1 Hz, aromatic-H), 7.90 (d, 1H, *J* = 8.0 Hz, isatin), 8.03 (d, 2H, *J* = 8.8 Hz, aromatic-H), 8.70 (s, 1H, -CH=N-, azomethine), 9.32 (s, 1H, pyrazole H-5), 10.79 (s, 1H, NH-isatin exchangeable with D<sub>2</sub>O); <sup>13</sup>C NMR (DMSO-*d*<sub>6</sub>, 126 MHz,  $\delta$  ppm) 111.02, 117.02, 117.15, 119.87, 122.75, 128.03, 129.25, 129.32, 129.45, 129.98, 130.17, 131.36, 132.37, 133.94, 139.38, 145.32, 151.50, 153.78, 157.24 (23C, 22C of aromatic + 1C of azomethine -N=CH-), 165.40 (1C, C=O); anal. calcd. (%) for C<sub>24</sub>H<sub>17</sub>N<sub>5</sub>O (391.42): C, 73.64; H, 4.38; N, 17.89. Found: C, 73.70; H, 4.33; N, 17.95%.

**5.2.10. 3-(((1-Phenyl-3-(4-methylphenyl)-1H-pyrazol-4-yl)methylene)hydrazono)indolin-2-one (5c).** Orange crystals; M.p.: 244–246 °C; yield (83%); IR (KBr)  $\nu_{\text{max}}/\text{cm}^{-1}$  3202 (NH), 1727 (C=O), 1615 (C=N), 1532 (C=C); <sup>1</sup>H NMR (DMSO-*d*<sub>6</sub>, 500 MHz,  $\delta$  ppm) 2.36 (s, 3H, CH<sub>3</sub>), 6.83 (d, 1H, *J* = 7.8 Hz, isatin), 6.88 (t, 1H, isatin), 7.34–7.30 (m, 3H, aromatic-H), 7.40 (t, 1H, isatin), 7.56 (t, 2H, aromatic-H), 7.62 (d, 2H, *J* = 8.0 Hz, aromatic-H), 7.90 (d, 1H, *J* = 7.4 Hz, isatin), 8.02 (d, 2H, *J* = 8.1 Hz, aromatic-H), 8.69 (s, 1H, -CH=N-, azomethine), 9.30 (s, 1H, pyrazole H-5), 10.78 (s, 1H, NH-isatin exchangeable with D<sub>2</sub>O); <sup>13</sup>C NMR (DMSO-*d*<sub>6</sub>, 126 MHz,  $\delta$  ppm) 21.00 (1C, CH<sub>3</sub>), 110.53, 116.41, 116.65, 119.33, 122.23, 127.52, 128.48, 128.72, 128.96, 129.36, 129.70, 130.79, 133.50, 138.50, 138.86, 144.80, 151.06, 153.38, 157.25 (23C, 22C of aromatic + 1C of azomethine -N=CH-), 164.94 (1C, C=O); anal. calcd. (%) for C<sub>25</sub>H<sub>19</sub>N<sub>5</sub>O (405.45): C, 74.06; H, 4.72; N, 17.27. Found: C, 74.00; H, 4.80; N, 17.35%.

**5.2.11. 3-(((3-(Benzofuran-2-yl)-1-phenyl-1H-pyrazol-4-yl)methylene)hydrazono)indolin-2-one (6).** Yellow crystals; M.p.: 274–276 °C; yield (89%); IR (KBr)  $\nu_{\text{max}}/\text{cm}^{-1}$  3197 (NH), 1717 (C=O), 1610 (C=N), 1566 (C=C); <sup>1</sup>H NMR (DMSO-*d*<sub>6</sub>, 500 MHz,  $\delta$  ppm) 6.88 (d, 1H, *J* = 8.2 Hz, isatin), 6.95 (t, 1H, isatin), 7.31 (t, 1H, aromatic-H), 7.38 (t, 2H, 1H of isatin and 1H of aromatic-H), 7.46 (t, 1H, aromatic-H), 7.59–7.63 (m, 3H, aromatic-H), 7.73 (d, 1H, *J* = 8.1 Hz, aromatic-H), 7.75 (d, 1H, *J* = 8.6 Hz, aromatic-H), 8.09 (d, 2H, *J* = 8.8 Hz, aromatic-H), 8.14 (d, 1H, *J* = 7.9 Hz, isatin), 9.06 (s, 1H, -CH=N-, azomethine), 9.40 (s, 1H, pyrazole H-5), 10.86 (s, 1H, NH-isatin exchangeable with D<sub>2</sub>O); <sup>13</sup>C NMR (DMSO-*d*<sub>6</sub>, 126 MHz,  $\delta$  ppm) 106.75, 111.17, 112.02, 117.09, 117.60, 120.00, 120.19, 122.23, 122.92, 124.09, 125.92, 128.45, 130.03, 130.23, 130.32, 130.71, 134.15, 139.21, 144.06, 145.48, 149.18, 151.32, 155.04 (25C, 24C of aromatic + 1C of azomethine -N=CH-), 164.94 (1C, C=O). Anal. calcd. (%) for C<sub>26</sub>H<sub>17</sub>N<sub>5</sub>O<sub>2</sub> (431.45): C, 72.38; H, 3.97; N, 16.23. Found: C, 72.45; H, 3.90; N, 16.30%.

**5.2.12. 3,3'-(((Methylenebis(oxy))bis(4,1-phenylene))bis(methanylylidene))bis(hydrazine-2,1-diylidene))bis(indolin-2-one) (7a).** Orange crystals, M.p.: 255–257 °C, yield (72%); IR (KBr)  $\nu_{\text{max}}/\text{cm}^{-1}$  3204 (NH), 1730 (C=O), 1605 (C=N), 1544 (C=C); <sup>1</sup>H NMR (DMSO-*d*<sub>6</sub>, 500 MHz,  $\delta$  ppm) 6.03 (d, 2H, -OCH<sub>2</sub>O-), 6.85 (d, 1H, *J* = 8.0 Hz, aromatic-H), 6.98–7.01 (t, 1H, *J* = 7.5 Hz, aromatic-H), 7.21 (t, 2H, *J* = 8.0 Hz, aromatic-H), 7.26–7.29 (m, 4H, aromatic-H), 7.37 (t, 2H, *J* = 7.5 Hz, aromatic-H), 7.78–7.83

(m, 2H, aromatic-H), 7.86–7.89 (m, 1H, aromatic-H), 7.94–7.96 (m, 3H, aromatic-H), 8.58, 8.61 (2s, 2H, 2-N=CH– azomethine), 10.81 (s, 2H, 2NH-isatin exchangeable with D<sub>2</sub>O); <sup>13</sup>C NMR (DMSO-*d*<sub>6</sub>, 126 MHz,  $\delta$  ppm): 89.38 (1C, CH<sub>2</sub>), 110.79, 116.68, 122.38, 127.75, 128.92, 130.09, 130.97, 131.82, 133.62, 144.94, 150.68, 159.19, 160.94 (28C, 26C of aromatic + 2C of azomethine –N=CH–), 164.67 (2C, 2C=O); anal. calcd. (%) for C<sub>31</sub>H<sub>22</sub>N<sub>6</sub>O<sub>4</sub> (542.54): C, 68.63; H, 4.09; N, 15.49. Found: C, 68.70; H, 4.03; N, 15.41%.

**5.2.13. 3,3'-(((Ethane-1,2-diylbis(oxy)))bis(4,1-phenylene))bis(methanylylidene))bis(hydrazine-2,1-diylidene))bis(indolin-2-one) (7b).** Yellow crystals, M.p.: 218–220 °C, yield (68%); IR (KBr)  $\nu_{\text{max}}/\text{cm}^{-1}$  3199 (NH), 1725 (C=O), 1607 (C=N), 1553 (C=C); <sup>1</sup>H NMR (DMSO-*d*<sub>6</sub>, 500 MHz,  $\delta$  ppm) 4.49 (s, 4H, –OCH<sub>2</sub>–CH<sub>2</sub>O–), 6.90 (d, 2H, *J* = 8.3 Hz, aromatic-H), 7.04 (t, 2H, aromatic-H), 7.11 (t, 2H, aromatic-H), 7.21 (d, 2H, *J* = 8.5 Hz, aromatic-H), 7.39 (t, 2H, aromatic-H), 7.83 (d, 2H, *J* = 8.1 Hz, aromatic-H), 7.97 (d, 2H, *J* = 8.0 Hz, aromatic-H), 8.05 (d, 2H, *J* = 7.4 Hz, aromatic-H), 8.56 (s, 2H, –N=CH–, azomethine), 10.85 (s, 2H, NH-isatin exchangeable with D<sub>2</sub>O); anal. calcd. (%) for C<sub>32</sub>H<sub>24</sub>N<sub>6</sub>O<sub>4</sub> (556.57): C, 69.06; H, 4.35; N, 15.10. Found: C, 69.00; H, 4.40; N, 15.00%.

### 5.3. *In vitro* biological activities

#### 5.3.1. Antioxidant activity

**5.3.1.1. Total antioxidant capacity.** Total antioxidant capacity (TAC) was determined by evaluating the green phosphate/Mo<sup>5+</sup> complex at wavelength 695 nm using the method described by Prieto *et al.*<sup>86</sup> It was expressed as mg gallic acid equivalent per gram dry weight (see ESI file†).

**5.3.1.2. Iron-reducing power.** Total iron-reducing power was assessed using the method suggested by Oyaizu<sup>87</sup> as  $\mu\text{g mL}^{-1}$ . A high absorbance of the reaction mixture at 700 nm indicates a higher reducing power (see ESI file†).

**5.3.1.3. DPPH radical-scavenging activity.** The scavenging activity against 1,1-diphenyl-2-picryl-hydrazyl (DPPH) radical was assayed by calculating the median inhibitory concentration (IC<sub>50</sub>) according to the method suggested<sup>88</sup> (see ESI file†).

**5.3.1.4. ABTS radical scavenging assay.** The 2,2'-azinobis-(3-ethylbenzothiazoline-6-sulfonic acid) (ABTS) assay was carried out to determine the percent of the ABTS radical inhibition (%) according to the method modified by Arnao *et al.*<sup>89</sup> using ascorbic acid as standard (see ESI file†).

**5.3.2. Anti-diabetic activity ( $\alpha$ -amylase inhibitory assay).** The anti-diabetic activity was assayed by  $\alpha$ -amylase inhibitory assay according to the 3,5-dinitrosalicylic acid (DNSA) method<sup>51</sup> for calculating the percentage of  $\alpha$ -amylase inhibition (%) using acarbose as a standard drug (see ESI file†).

**5.3.3. Anti-alzheimer activity (acetylcholinesterase (AChE) enzyme inhibition).** The anti-Alzheimer activity was measured by calculating the percentage of acetylcholinesterase (AChE) enzyme inhibition (%) according to Ellman's method<sup>53</sup> (see ESI file†).

#### 5.3.4. Anti-arthritis activity

**5.3.4.1. Protein denaturation.** The percentage of protein denaturation inhibition was calculated according to the

reported method.<sup>90</sup> and modified by Soni and Sureshkumar.<sup>91</sup> All results were compared with the standard (diclofenac sodium) that was prepared according to the method described.<sup>92</sup> The control represents 100% protein denaturation (see ESI file†).

**5.3.4.2. Proteinase inhibitory activity.** This assay was carried out by calculating the percentage of the proteinase inhibitory activity was according to the method suggested<sup>93</sup> (see ESI file†).

### 5.4. Statistical analysis

The statistical positive and negative correlations were evaluated among measurements of the biological activities using one-way analysis of variance (oneway ANOVA) by Statistical Package for Social Sciences (SPSS for windows, version 11.0). Values of *P* < 0.05 were considered significant correlation and those of *P* < 0.01 were considered highly significant one.

### 5.5. Density function theory (DFT) calculation

The fully geometry optimized for the most active derivatives **3b**, **5a**, **5b**, and **5c** was performed using the Gaussview 6.0 and Gaussian 09<sup>94</sup> at the DFT/B3LYP 6–31 g (d) basis set, in gas phase for all atoms as described previously.<sup>64,69</sup>

### 5.6. Molecular docking simulation

The molecular docking simulation was performed inside the active site of human pancreatic  $\alpha$ -amylase complexed with co-crystallized ligand acarbose ( $\alpha$ -amylase PDB: 2QV4) was selected for antidiabetic activity. Further, the recombinant human acetylcholinesterase (AChE) (PDB: 4EY7) was used for anti-Alzheimer's activity. The crystal structures of these two proteins were downloaded from the protein data bank (<https://www.rcsb.org/>) and the active site was generated as described previously<sup>73</sup> using Molecular Operating Environment (MOE) software version 2009  $\times 10$ .<sup>95–97</sup> In addition, target compound structures were generated with ChemBioDraw 2014, exported to MOE, where hydrogen atoms were added, and structures were minimized with MMFF94X forcefield using 0.001 RMS kcal mol<sup>–1</sup><sup>98,99</sup> (all details are represented in ESI file†).

### 5.7. *In silico* studies

The physicochemical properties and drug-likeness of isatin-based Schiff bases **3b** and **5a–c** were calculated using SwissADME website <http://www.swissadme.ch/index.php>.<sup>74</sup> While the Drug-likeness scores were calculated using Molsoft LLC website <https://www.molsoft.com/mprop/>.<sup>75</sup> The toxic properties were calculated using ADMETlab 2.0 website <https://admetmesh.scbdd.com/service/evaluation/cal>.<sup>80</sup> But the metabolism properties was computed using the pkCSM-pharmacokinetics website <https://biosig.lab.uq.edu.au/pkcsm/prediction><sup>81</sup> also the probability value (the range of zero to one) of the metabolism properties, the absorption, and distribution properties were calculated using ADMETlab 2.0 website <https://admetmesh.scbdd.com/service/evaluation/cal>.<sup>84</sup>



## Conflicts of interest

The authors declare that they have no known competing financial interests or personal relationships that could have appeared to influence the work reported in this paper.

## Acknowledgements

The authors wish to thank the National Research Centre for the facilities provided.

## References

- 1 J. Ahmad Malik, S. Ahmed, M. Shinde, M. H. S. Almermesh, S. Alghamdi, A. Hussain and S. Anwar, *Saudi J. Biol. Sci.*, 2022, **29**, 3586–3599.
- 2 J. Dowarah and V. P. Singh, *Bioorg. Med. Chem.*, 2020, **28**, 115263.
- 3 N. Oumata, K. Lu, Y. Teng, C. Cavé, Y. Peng, H. Galons and B. P. Roques, *Eur. J. Med. Chem.*, 2022, **240**, 114578.
- 4 D. J. Selkoe, *Ann. N. Y. Acad. Sci.*, 2000, **924**, 17–25.
- 5 Z. Breijyeh and R. Karaman, *Molecules*, 2020, **25**, 5789.
- 6 Alzheimer's Association, *Alzheimer's Assoc. Rep.*, 2019, vol. 15, pp. 321–387.
- 7 A. A. Alhazzani, M. Alqahtani, A. Alshbriqe, A. Awwadh, T. Alyami, M. Alshomrani and O. A. Mostafa, *J. Neurol. Sci.*, 2017, **381**, 315.
- 8 C. G. Lyketsos and J. Olin, *Biol. Psychiatry*, 2002, **52**, 243–252.
- 9 S. Gauthier, J. Cummings, C. Ballard, H. Brodaty, G. Grossberg, P. Robert and C. Lyketsos, *Int. Psychogeriatr.*, 2010, **22**, 346–372.
- 10 D. Harman, *Ann. N. Y. Acad. Sci.*, 2001, **928**, 1–21.
- 11 L. Zhu, M. Luo, Y. Zhang, F. Fang, M. Li, F. An, D. Zhao and J. Zhang, *Coord. Chem. Rev.*, 2023, **475**, 214875.
- 12 B. Akbari, N. Baghaei-Yazdi, M. Bahmaie and F. Mahdavi Abhari, *BioFactors*, 2022, **48**, 611–633.
- 13 E. Jaul and J. Barron, *Front. Public Health*, 2017, **5**, 335.
- 14 S. K. Beura, R. Dhapola, A. R. Panigrahi, P. Yadav, D. H. Reddy and S. K. Singh, *Life Sci.*, 2022, **306**, 120855.
- 15 C. Huang, J. Luo, X. Wen and K. Li, *Biochem. Genet.*, 2022, **60**, 1049–1075.
- 16 X. Xia, Q. Jiang, J. McDermott and J. D. J. Han, *Aging Cell*, 2018, **17**, e12802.
- 17 Z. Haghighijoo, L. Zamani, F. Moosavi and S. Emami, *Eur. J. Med. Chem.*, 2022, **227**, 113949.
- 18 S. Gupta, V. Singh, P. K. Varadwaj, N. Chakravartty, A. V. S. K. M. Katta, S. P. Lekkala, G. Thomas, S. Narasimhan, A. R. Reddy and V. B. Reddy Lachagari, *J. Biomol. Struct. Dyn.*, 2022, **40**, 2264–2283.
- 19 A. Kabir and A. Muth, *Pharmacol. Res.*, 2022, **176**, 106055.
- 20 X. H. Makhoba, C. Viegas, R. A. Mosa, F. P. D. Viegas and O. J. Poee, *Drug Des., Dev. Ther.*, 2020, **14**, 3235–3249.
- 21 E. G. Guzman-Lopez, M. Reina, A. Perez-Gonzalez, M. Francisco-Marquez, L. F. Hernandez-Ayala, R. Castañeda-Arriaga and A. Galano, *Int. J. Mol. Sci.*, 2022, **23**, 13246.
- 22 A. Pérez-González, R. Castañeda-Arriaga, E. G. Guzmán-López, L. F. Hernández-Ayala and A. Galano, *ACS Omega*, 2022, **7**, 38254–38268.
- 23 M. G. A. Al-Khuzai, M. M. Fahad and A. J. Al-Safi, *Biomed. Chem. Sci.*, 2022, **3**, 193–206.
- 24 R. S. Cheke, V. M. Patil, S. D. Firke, J. P. Ambhore, I. A. Ansari, H. M. Patel, S. D. Shinde, V. R. Pasupuleti, M. I. Hassan, M. Adnan, A. Kadri and M. Snoussi, *Pharmaceuticals*, 2022, **15**, 272.
- 25 B. D. Varpe, A. A. Kulkarni, S. B. Jadhav, A. S. Mali and S. Y. Jadhav, *Mini-Rev. Med. Chem.*, 2020, **21**, 1182–1225.
- 26 I. Abbasi, H. Nadeem, A. Saeed, H. A. A. Kharl, M. N. Tahir and M. M. Naseer, *Bioorg. Chem.*, 2021, **116**, 105385.
- 27 B. Mavroidi, A. Kaminari, D. Matiadis, D. Hadjipavlou-Litina, M. Pelecanou, A. Tzinia and M. Sagnou, *Brain Sci.*, 2022, **12**, 806.
- 28 I. Tumosienė, I. Jonuškienė, K. Kantminienė, V. Mickevičius and V. Petrikaitė, *Int. J. Mol. Sci.*, 2021, **22**, 7799.
- 29 A. M. S. El-Sharief, Y. A. Ammar, A. Belal, M. A. M. S. El-Sharief, Y. A. Mohamed, A. B. M. Mehany, G. A. M. Elhag Ali and A. Ragab, *Bioorg. Chem.*, 2019, **85**, 399–412.
- 30 M. A. Salem, A. Ragab, A. El-Khalafawy, A. H. Makhlof, A. A. Askar and Y. A. Ammar, *Bioorg. Chem.*, 2020, **96**, 103619.
- 31 Y. A. Ammar, A. M. Sh El-Sharief, A. Belal, S. Y. Abbas, Y. A. Mohamed, A. B. M. Mehany and A. Ragab, *Eur. J. Med. Chem.*, 2018, **156**, 918–932.
- 32 S. A. El-Kalyoubi, A. Ragab, O. A. Abu Ali, Y. A. Ammar, M. G. Seadawy, A. Ahmed and E. A. Fayed, *Pharmaceuticals*, 2022, **15**, 376.
- 33 A. S. Hassan, G. O. Moustafa, H. M. Awad, E. S. Nossier and M. F. Mady, *ACS Omega*, 2021, **6**, 12361–12374.
- 34 S. H. Sumrra, W. Zafar, M. L. Asghar, F. Mushtaq, M. A. Raza, M. F. Nazar, M. A. Nadeem, M. Imran and S. Mumtaz, *J. Mol. Struct.*, 2021, **1238**, 130382.
- 35 A. S. Hassan, A. A. Askar, A. M. Naglah, A. A. Almehizia and A. Ragab, *Molecules*, 2020, **25**, 2593.
- 36 A. M. Abdelghany, T. K. Khatab and A. S. Hassan, *Bull. Chem. Soc. Ethiop.*, 2021, **35**, 185–196.
- 37 H. R. Elgiushy, S. H. Mohamed, H. Taha, H. Sawaf, Z. Hassan, N. A. Abou-Taleb, E. M. El-labbad, A. S. Hassan, K. A. M. Abouzid and S. F. Hammad, *Bioorg. Chem.*, 2022, **120**, 105646.
- 38 A. S. Hassan, *Bull. Chem. Soc. Ethiop.*, 2020, **34**, 533–541.
- 39 A. S. Hassan, D. M. Masoud, F. M. Sroor and A. A. Askar, *Med. Chem. Res.*, 2017, **26**, 2909–2919.
- 40 A. S. Hassan, S. A. Osman and T. S. Hafez, *Egypt. J. Chem.*, 2015, **58**, 113–139.
- 41 M. Eldeeb, E. F. Sanad, A. Ragab, Y. A. Ammar, K. Mahmoud, M. M. Ali and N. M. Hamdy, *Biomedicines*, 2022, **10**, 722.
- 42 M. M. Abdelgalil, Y. A. Ammar, G. A. M. Elhag Ali, A. K. Ali and A. Ragab, *J. Mol. Struct.*, 2023, **1274**, 134443.
- 43 A. El-Faham, A. A. Elzatahry, Z. A. Al-Othman and E. A. Elsayed, *Int. J. Nanomed.*, 2014, **9**, 1167–1174.
- 44 N. M. Morsy, A. S. Hassan, T. S. Hafez, M. R. H. Mahran, I. A. Sadawe and A. M. Gbaj, *J. Iran. Chem. Soc.*, 2021, **18**, 47–59.





- 45 G. Yapar, N. Demir, A. Kiraz, G. Y. Özkut and M. Yıldız, *J. Mol. Struct.*, 2022, **1266**, 133530.
- 46 M. M. J. Al-Mudhafar, T. N.-A. Omar and S. L. Abdulhadi, *Al Mustansiriyah J. Pharm. Sci.*, 2022, **22**, 23–48.
- 47 S. Daoud, S. Thiab, T. M. A. Jazzazi, T. M. A. Al-Shboul and S. Ullah, *Acta Pharm.*, 2022, **72**, 449–458.
- 48 S. H. Sumrra, S. Kausar, M. A. Raza, M. Zubair, M. N. Zafar, M. A. Nadeem, E. U. Mughal, Z. H. Chohan, F. Mushtaq and U. Rashid, *J. Mol. Struct.*, 2018, **1168**, 202–211.
- 49 Y. Liu, F. Wen, H. Yang, L. Bao, Z. Zhao and Z. Zhong, *Heliyon*, 2022, **8**, e10624.
- 50 W. L. Henry, *J. Natl. Med. Assoc.*, 1962, **54**, 476–478.
- 51 M. N. Wickramaratne, J. C. Punchihewa and D. B. M. Wickramaratne, *BMC Complementary Altern. Med.*, 2016, **16**, 466.
- 52 M. Goschorska, I. Gutowska, I. Baranowska-Bosiacka, K. Piotrowska, E. Metryka, K. Safranow and D. Chlubek, *Int. J. Environ. Res. Public Health*, 2019, **16**, 10.
- 53 G. L. Ellman, K. D. Courtney, V. Andres and R. M. Featherstone, *Biochem. Pharmacol.*, 1961, **7**, 88–95.
- 54 B. Balraj, N. Senthikumar, I. Vetha Potheher and M. Arulmozhi, *Mater. Sci. Eng., B*, 2018, **231**, 121–127.
- 55 N. I. Osman, N. J. Sidik, A. Awal, N. A. M. Adam and N. I. Rezali, *J. Intercult. Ethnopharmacol.*, 2016, **5**, 343–349.
- 56 V. S. Djova, A. M. Nyegue and F.-X. Etoa, *J. Drug Delivery Ther.*, 2018, **8**, 174–181.
- 57 R. Ayman, A. M. Radwan, A. M. Elmetwally, Y. A. Ammar and A. Ragab, *Arch. Pharm.*, 2023, **356**, e2200395.
- 58 R. Thirumalaisamy, F. Ameen, A. Subramanian, T. Selvankumar, S. S. Alwakeel and M. Govarthanan, *Int. J. Pept. Res. Ther.*, 2020, **26**, 2179–2189.
- 59 P. Shah and A. D. Westwell, *J. Enzyme Inhib. Med. Chem.*, 2007, **22**, 527–540.
- 60 B. M. Johnson, Y. Z. Shu, X. Zhuo and N. A. Meanwell, *J. Med. Chem.*, 2020, **63**, 6315–6386.
- 61 S. S. Mukhtar, A. S. Hassan, N. M. Morsy, T. S. Hafez, F. M. Saleh and H. M. Hassaneen, *Synth. Commun.*, 2021, **51**, 1564–1580.
- 62 D. Russo, P. Valentão, P. B. Andrade, E. C. Fernandez and L. Milella, *Int. J. Mol. Sci.*, 2015, **16**, 17696–17718.
- 63 A. Y. Alzahrani, Y. A. Ammar, M. A. Salem, M. Abu-Elghait and A. Ragab, *Arch. Pharm.*, 2022, **355**, e2100266.
- 64 A. Y. Alzahrani, Y. A. Ammar, M. Abu-Elghait, M. A. Salem, M. A. Assiri, T. E. Ali and A. Ragab, *Bioorg. Chem.*, 2022, **119**, 105571.
- 65 D. M. Elsis, A. Ragab, A. A. Elhenawy, A. A. Farag, A. M. Ali and Y. A. Ammar, *J. Mol. Struct.*, 2022, **1247**, 131314.
- 66 R. Ayman, M. S. Abusaif, A. M. Radwan, A. M. Elmetwally and A. Ragab, *Eur. J. Med. Chem.*, 2023, **249**, 115138.
- 67 A. Ragab, M. S. Abusaif, N. A. Gohar, D. S. Aboul-Magd, E. A. Fayed and Y. A. Ammar, *Bioorg. Chem.*, 2023, **131**, 106307.
- 68 A. Ragab, M. S. Abusaif, D. S. Aboul-Magd, M. M. S. Wassel, G. A. M. Elhagali and Y. A. Ammar, *Drug Dev. Res.*, 2022, **1305**–1330.
- 69 K. E. Saadon, N. M. H. Taha, N. A. Mahmoud, G. A. M. Elhagali and A. Ragab, *J. Iran. Chem. Soc.*, 2022, **19**, 3899–3917.
- 70 A. Ragab, Y. A. Ammar, A. Ezzat, A. M. Mahmoud, M. B. I. Mohamed, A. S. El-Tabl and R. S. Farag, *Comput. Biol. Med.*, 2022, **145**, 105473.
- 71 E. S. A. E. H. Khattab, A. Ragab, M. A. Abol-Ftouh and A. A. Elhenawy, *J. Biomol. Struct. Dyn.*, 2022, **40**, 1–19.
- 72 S. A. Ibrahim, A. Ragab and H. A. El-Ghamry, *Appl. Organomet. Chem.*, 2022, **36**, e6508.
- 73 A. S. Hassan, N. M. Morsy, W. M. Aboulthana and A. Ragab, *Drug Dev. Res.*, 2023, **84**, 3–24.
- 74 A. M. Naglah, A. A. Askar, A. S. Hassan, T. K. Khatab, M. A. Al-Omar and M. A. Bhat, *Molecules*, 2020, **25**, 1431.
- 75 A. S. Hassan, N. M. Morsy, H. M. Awad and A. Ragab, *J. Iran. Chem. Soc.*, 2022, **19**, 521–545.
- 76 F. Zhao, P. Wang, Y. Jiao, X. Zhang, D. Chen and H. Xu, *Front. Pharmacol.*, 2020, **11**, 579332.
- 77 A. Daina, O. Michielin and V. Zoete, *Sci. Rep.*, 2017, **7**, 42717.
- 78 A. S. Al Wasidi, A. S. Hassan and A. M. Naglah, *J. Appl. Pharm. Sci.*, 2020, **10**, 142–148.
- 79 E. M. Gad, M. S. Nafie, E. H. Eltamany, M. S. A. G. Hammad, A. Barakat, A. Barakat and A. T. A. Boraei, *Molecules*, 2020, **25**, 2523.
- 80 G. Xiong, Z. Wu, J. Yi, L. Fu, Z. Yang, C. Hsieh, M. Yin, X. Zeng, C. Wu, A. Lu, X. Chen, T. Hou and D. Cao, *Nucleic Acids Res.*, 2021, **49**, W5–W14.
- 81 A. S. Hassan, *J. Iran. Chem. Soc.*, 2022, **19**, 3577–3589.
- 82 J. Hakkola, J. Hukkanen, M. Turpeinen and O. Pelkonen, *Arch. Toxicol.*, 2020, **94**, 3671–3722.
- 83 Y. Wang, J. Xing, Y. Xu, N. Zhou, J. Peng, Z. Xiong, X. Liu, X. Luo, C. Luo, K. Chen, M. Zheng and H. Jiang, *Q. Rev. Biophys.*, 2015, **48**, 488–515.
- 84 N. N. Wang, J. Dong, Y. H. Deng, M. F. Zhu, M. Wen, Z. J. Yao, A. P. Lu, J. B. Wang and D. S. Cao, *J. Chem. Inf. Model.*, 2016, **56**, 763–773.
- 85 M. L. Amin, *Drug Target Insights*, 2013, **2013**, 27–34.
- 86 P. Prieto, M. Pineda and M. Aguilar, *Anal. Biochem.*, 1999, **269**, 337–341.
- 87 M. Oyaizu, *Jpn. J. Nutr. Diet.*, 1986, **44**, 307–315.
- 88 M. M. Rahman, M. B. Islam, M. Biswas and A. H. M. Khurshid Alam, *BMC Res. Notes*, 2015, **8**, 621.
- 89 M. B. Arnao, A. Cano and M. Acosta, *Food Chem.*, 2001, **73**, 239–244.
- 90 P. Shivanand, *Int. J. Pharm. Life Sci.*, 2010, **1**, 38–43.
- 91 D. Soni and P. Sureshkumar, *Res. J. Biotechnol.*, 2016, **11**, 4.
- 92 S. Meera, N. Ramaiah and N. Kalidindi, *Saudi Pharm. J.*, 2011, **19**, 279–284.
- 93 O. O. Oyedapo and A. J. Famurewa, *Int. J. Pharmacogn.*, 1995, **33**, 65–69.
- 94 J. P. Foster and F. Weinhold, *J. Am. Chem. Soc.*, 1980, **102**, 7211–7218.
- 95 H. F. Rizk, M. A. El-Borai, A. Ragab, S. A. Ibrahim and M. E. Sadek, *Polycyclic Aromat. Compd.*, 2023, **43**, 500–522.



- 96 A. Ezzat, M. B. I. Mohamed, A. M. Mahmoud, R. S. Farag, A. S. El-Tabl and A. Ragab, *J. Mol. Struct.*, 2022, **1251**, 132004.
- 97 E. A. Fayed, M. Mohsen, S. M. A. El-Gilil, D. S. Aboul-Magd and A. Ragab, *J. Mol. Struct.*, 2022, **1262**, 133028.
- 98 Y. A. Ammar, J. A. Micky, D. S. Aboul-Magd, S. M. A. Abd El-Hafez, S. A. Hessein, A. M. Ali and A. Ragab, *Chem. Biol. Drug Des.*, 2023, **101**, 245–270.
- 99 H. Ali Mohamed, Y. A. Ammar, G. A. M. Elhagali, H. A. Eyada, D. S. Aboul-Magd and A. Ragab, *ACS Omega*, 2022, **7**, 4970–4990.

